Structural Elucidation of a Protective B cell Epitope on Outer Surface Protein C (OspC) of the Lyme disease spirochete, *Borreliella burgdorferi*

Michael J. Rudolph[1,*], Simon A. Davis[1], H M Emranul Haque[2], David D. Weis[2], David J Vance[3], Carol Lyn Piazza[3], Monir Ejemel[4], Lisa Cavacini[4], Yang Wang[4], M. Lamine Mbow[5,#], Robert D. Gilmore[5], and Nicholas J Mantis[3,*]

[1]New York Structural Biology Center, New York, NY; [2]Department of Chemistry, University of Kansas, Lawrence, KS; [3]Division of Infectious Diseases, Wadsworth Center, New York State Department of Health, Albany, NY; [4]MassBiologics of the University of Massachusetts Chan Medical School, Boston, MA; [5]Division of Vector Borne Diseases, National Center for Emerging and Zoonotic Infectious Diseases, Centers for Disease Control and Prevention, Fort Collins, CO, United States

[#], present address: Boehringer Ingelheim Pharmaceuticals, Ridgefield, CT 06877

*, Co-corresponding authors

Running title: Protective epitope on OspC

ABSTRACT

Outer surface protein C (OspC) plays a pivotal role in mediating tick-to-host transmission and infectivity of the Lyme disease spirochete, *Borreliella burgdorferi*. OspC is a helical-rich homodimer that interacts with tick salivary proteins, as well as components of the mammalian immune system. Several decades ago, it was shown that the OspC-specific monoclonal antibody, B5, was able to passively protect mice from experimental tick-transmitted infection by *B. burgdorferi* strain B31. However, B5's epitope has never been elucidated, despite widespread interest in OspC as a possible Lyme disease vaccine antigen. Here we report the crystal structure of B5 antigen-binding fragments (Fabs) in complex with recombinant OspC type A ($OspC_A$). Each OspC monomer within the homodimer was bound by a single B5 Fab in a side-on orientation, with contact points along OspC's α-helix 1 and α-helix 6, as well as interactions with the loop between α-helices 5 and 6. In addition, B5's complementarity-determining region (CDR) H3 bridged the OspC-OspC' homodimer interface, revealing the quaternary nature of the protective epitope. To provide insight into the molecular basis of B5 serotype specificity, we solved the crystal structures of recombinant OspC types B and K and compared them to $OspC_A$. This study represents the first structure of a protective B cell epitope on OspC and will aid in the rational design of OspC-based vaccines and therapeutics for Lyme disease.

IMPORTANCE

The spirochete, *Borreliella burgdorferi*, is the causative agent of Lyme borreliosis, the most common tickborne disease in the United States. The spirochete is transmitted to humans during the course of a tick taking a bloodmeal. After *B. burgdorferi* is deposited into the skin of a human host, it replicates locally and spreads systemically, often resulting in clinical manifestations involving the central nervous system, joints, and/or heart. Antibodies directed against *B. burgdorferi*'s outer surface protein C (OspC) are known to block tick-to-host transmission, as well as dissemination of the spirochete within a mammalian host. In this report, we reveal the first atomic structure of one such antibody in complex with OspC. Our results have implications for the design of a Lyme disease vaccine capable to interfering with multiple stages in *B. burgdorferi* infection.

Introduction

Borreliella burgdorferi is the principal etiological agent of Lyme disease (LD), the most common tick-borne infection in North America and Europe. In the United States, the vector of *B. burgdorferi* is the blacklegged ticks, *Ixodes scapularis* and *Ixodes pacificus*. Naïve larvae acquire *B. burgdorferi* during a blood meal on an infected reservoir species, including birds and an array of small mammals. Once within a tick, the spirochetal bacteria remain dormant in the midgut until a second blood meal taken during the nymphal stage, after which *B. burgdorferi* migrates to the salivary glands where it is deposited into the skin of an impending host. Perpetuation of *B. burgdorferi*'s enzoonotic cycle and persistence within vertebrate reservoirs is contingent on the spirochete's ability to evade innate and adaptive immunity (Di et al., 2022; Rana et al., 2022). Although humans are incidental ("dead end") hosts for *B. burgdorferi*, the spirochetes have the capacity to disseminate and colonize distal tissues, which contributes to the clinical manifestations commonly associated with Lyme disease, including erythema migrans, neuroborreliosis, carditis, and Lyme arthritis (Radolf et al., 2021; Steere et al., 2016). With an estimated 476,000 cases of Lyme disease per year in the United States (Kugeler et al., 2021), there is an urgent need for vaccines that prevent *B. burgdorferi* transmission and limit human infections (Dattwyler and Gomes-Solecki, 2022; Gomes-Solecki et al., 2020; Wormser, 2022).

Outer surface protein C (OspC) has long been considered a candidate Lyme disease vaccine antigen. OspC is a ~23 kDa helical-rich lipoprotein expressed by *B. burgdorferi* in the tick midgut during the course of a blood meal (Caimano et al., 2019; Eicken et al., 2001; Kumaran et al., 2001; Ohnishi et al., 2001; Schwan et al., 1995; Zuckert et al., 2001). OspC facilitates migration of *B. burgdorferi* from the midgut to the salivary glands and contributes to early stages of mammalian survival (De Silva and Fikrig, 1995; Ohnishi *et al.*, 2001; Pal et al., 2004; Schwan *et al.*, 1995). In the mouse model, OspC antibodies elicited through active or passive vaccination prevent tick-mediated *B. burgdorferi* infection (Gilmore et al., 1996; Mbow et al., 1999). Recent evidence indicates OspC antibodies entrap *B. burgdorferi* within the tick midgut by a mechanism that does not involve direct spirochete killing (Bhatia et al., 2018). OspC antibodies also protect mice against *B. burgdorferi* needle infection and have been reported to promote resolution of arthritis and carditis in SCID mouse model of Lyme disease (Gilmore *et al.*, 1996; Preac-Mursic et al., 1992; Probert and LeFebvre, 1994; Zhong et al., 1997). Thus,

OspC antibodies afford a double layer of protection by interfering with *B. burgdorferi* tick-to-host transmission and promoting clearance of spirochetes that do gain access to a mammalian host.

A major limitation of OspC as a vaccine antigen is its polymorphism within and across *B. burgdorferi* genospecies. At least 25 different *ospC* alleles or types have been identified to date, with extensive diversity occurring even within limited geographical regions (Baum et al., 2013; Bunikis et al., 2004; Earnhart et al., 2005; Hanincova et al., 2013; Seinost et al., 1999; Wang et al., 1999). The degree of OspC variability is such that antibody responses to a given OspC type have limited cross-reactivity with other OspC types (Barbour and Travinsky, 2010; Bhatia *et al.*, 2018; Bockenstedt et al., 1997). This is consequential because the immunodomnant nature of OspC and that susceptibility to *B. burgdorferi* re-infection and repeated episodes of Lyme disease has been linked to OspC variability (Baum *et al.*, 2013; Bhatia *et al.*, 2018; Bockenstedt *et al.*, 1997; Di *et al.*, 2022; Gilmore *et al.*, 1996; Nadelman et al., 2012; Rousselle et al., 1998). Thus, a vaccine based on a single OspC type would have limited utility in regions where multiple *B. burgdorferi* OspC types co-exist.

A multivalent or chimeric OspC vaccine consisting of conserved or minimally variable epitopes might afford protection against diverse *B. burgdorferi* strains (Izac and Marconi, 2019). The structures of OspC types A, I and E were solved two decades ago and revealed a high degree of tertiary and quaternary similarity (**Table 1; Figure S1**) (Eicken *et al.*, 2001; Kumaran *et al.*, 2001). In each case, OspC consisted of four long α-helices (1, 2, 3, 6), two shorter α–helices (4 and 5), and two short anti-parallel β-strands located between α1 and α2 (Eicken *et al.*, 2001; Kumaran *et al.*, 2001). The biologically functional molecule is a dimer (with monomers referred to as OspC-OspC' herein) that assumes a knob-shaped structure anchored via N-terminal lipidated moieties in the spirochete's outer surface membrane (Eicken *et al.*, 2001; Kumaran *et al.*, 2001; Zuckert *et al.*, 2001). The C-terminus of OspC folds back onto the rest of the molecule such that α-helix 6 runs antiparallel to α-helix 1 and terminates at the bacterial surface. Multiple sequence alignment (MSA) of 23 OspC proteins revealed blocks of conserved residues localized in the N- (residues ~31-78) and C-termini (residues ~191-206), whereas high degrees of variably are within the short anti-parallel β-strands and other patches throughout the molecule (Baum *et al.*, 2013; Earnhart *et al.*, 2005; Earnhart et al., 2010; Earnhart and Marconi, 2007; Wilske et al., 1992). Computational modeling and linear B cell epitope analysis has identified regions on OspC

likely to be the major determinants of type-specific and cross-reactive antibody recognition (Baum *et al.*, 2013; Earnhart *et al.*, 2005; Earnhart *et al.*, 2010; Earnhart and Marconi, 2007; Izac et al., 2019; Izac et al., 2020; Wilske *et al.*, 1992). However, no structure of a conformational (non-linear) protective epitope on OspC has been reported to date.

B5 is an OspC-specific mouse monoclonal IgG antibody (MAb) first identified in a screen of B cell hybridomas from mice infected with *B. burgdorferi* strain B31 (Mbow et al., 2002). Passive immunization studies demonstrated that B5 IgG is sufficient to protect mice against experimental tick-mediated *B. burgdorferi* challenge, possibly by interfering with spirochete egress from the tick midgut (Gilmore and Piesman, 2000; Mbow *et al.*, 1999). B5 IgG remains the only OspC MAb to have been shown to be protective against natural route of *B. burgdorferi* transmission, making it a valuable reagent to understand the molecular mechanism of OspC antibody function towards *B. burgdorferi*. In this study, we report the X-ray crystal of B5 Fab fragments in complex with an $OspC_A$ homodimer. The structure represents the first elucidation of a protective epitope on OspC and unveils molecular interactions that constrain the breadth of B5 reactivity across OspC types.

Results and Discussion

B5 IgG was originally isolated from mice that had been experimentally challenged with *B. burgdorferi* strain B31 (Gilmore and Mbow, 1999; Mbow *et al.*, 1999). Due to limited supply of mouse B5 IgG, we generated a recombinant chimeric derivative of B5 in which murine V_H and V_L elements were fused to human IgG_1 Fc and kappa light chains and expressed in Expi293 cells. Using purified mouse B5 IgG as well as the chimeric-derivative of B5 IgG1, we confirmed B5 reactivity with OspC. Recognition of native OspC on the surface of viable spirochetes was demonstrated by flow cytometry: a derivative *B. burgdorferi* strain B31 was incubated with B5 IgG or an isotype control (PB10 IgG) followed by Alexa647-labeled secondary antibody then analyzed for mean fluorescence intensity (MFI). B5 IgG labeled >80% of the live spirochetes with an MFI >3200, as compared to the isotype control, which labeled <1% of cells with MFI of ~50 (**Figure 1A,B**). To assess the breadth of B5 IgG reactivity, ELISA plates coated with recombinant $OspC_A$, OspC type B ($OspC_B$) and K ($OspC_K$), then probed with a range of B5 IgG concentrations. By ELISA, B5 IgG reacted exclusively with $OspC_A$, indicating that the MAb has limited OspC cross reactivity (**Figure 1C**). Similar results were observed by dot blot (**Figure**

1D). Using biolayer inferometry (BLI), B5 IgG had an apparent dissociation constant (K_D) of ~ 0.2 nM for recombinant $OspC_A$ (**Figure S2**). These results confirm that B5 IgG recognizes both native and recombinant $OspC_A$.

B5 IgG epitope localization using hydrogen exchange-mass spectrometry (HX-MS). It was previously reported that B5 IgG recognizes a conformationally-sensitive epitope on OspC, possibly involving the C-terminus of α-helix 6 (Gilmore and Mbow, 1999). To localize B5 IgG's epitope in more detail, recombinant $OspC_A$ was subjected to HX-MS in the absence and presence of mouse B5 IgG. HX-MS provides peptide level resolution of antibody-antigen interactions in solution based on differential hydrogen-deuterium exchange rates between unbound and bound targets (Angalakurthi et al., 2018; Brier et al., 2021; Chen et al., 2019; Grauslund et al., 2021; Hodge et al., 2022; Malito et al., 2013; Seow et al., 2022; Vinciauskaite and Masson, 2022). We recently used HX-MS to localize a dozen human B cell epitopes the *B. burgdorferi* antigen, OspA (Haque et al., 2022). In the case of OspC, we first generated a peptidic map of $OspC_A$, which yielded 87 peptides that covered the entire length of the molecule (**Figure S3**). By HX-MS, the OspC N- and C-terminal regions displayed a high degree of flexibility in the unbound state, as evidenced by a high degree of exchange (**data not shown**). The addition of B5 IgG resulted in weak, but statistically significant protection across the majority of the OspC molecule, possibly reflecting a combination of allosteric effects and dynamic interconversion between bound and unbound states of the antigen. The strongest protection, however, encompassed $OspC_A$'s terminal α-helix 6, corresponding to peptidic residues 163-168, 171-172, 174-175, 177-179, 181-182, 184-186, 188-197, and 199-200 (**Figure 2**). These results suggest that binding of B5 IgG influences flexibility of the entire length of OspC's terminal α-helix.

X-ray crystal structure of Fab B5-$OspC_A$. To define B5's epitope in greater detail, we solved the X-ray crystal structure of the B5 Fab fragment in complex with $OspC_A$ at 2.7 Å resolution in the $P2_12_12$ space group. The crystal structure revealed two B5 Fabs bound to a single $OspC_A$ homodimer (1:1 Fab:$OspC_A$ stoichiometry) in a side-on fashion (**Figure 3**). The B5 Fab fragments (Fab, Fab') made nearly identical contacts on opposite sides of the $OspC_A$ homodimer, as described in detail below. B5 Fabs assumed a canonical structure with two heavy chain immunoglobulin domains (V_H, C_H1) and two light immunoglobulin domains (V_L, C_L) each containing 7-10 β-strands arranged in two β-sheets that folded into a two-layer sandwich with all six CDRs (L1-3, H1-3) on one face of the molecule. The homodimeric structure of $OspC_A$

unbound [PDB 1GGQ] and bound to B5 Fabs were similar, as evidenced by a Root-Mean-Square Deviation (RMSD) of 1.0 Å. Thus, antibody engagement did not induce any major conformational changes $OspC_A$.

The interaction between B5 Fab and $OspC_A$ buried a total surface area of 2,040 $Å^2$ (2,002 $Å^2$ for the second B5-$OspC_A$ interface within the asymmetric unit) establishing nine hydrogen bonds and three salt bridges (12 hydrogen bonds and three salt bridges for the second B5-$OspC_A$ interface within the asymmetric unit) (**Table 2**; **Figure 4**). The B5 Fab V_H domain contributed slightly more to the interaction burying 1042 $Å^2$ (1027 $Å^2$ for the second B5-$OspC_A$ contact within the asymmetric unit) than the V_L domain which buried 998 $Å^2$ (975 $Å^2$ for the second B5-$OspC_A$ interface in the asymmetric unit). The B5 V_H domain formed four hydrogen bonds (three hydrogen bonds for the second B5-$OspC_A$ interface in the asymmetric unit) that includes CDR-H1 residue Tyr-27 with $OspC_A$ Lys-175, and CDR-H3 residue Tyr-102 and $OspC_A$ Glu-71 (**Figure 4**). The B5 V_H domain also accounted for two of the three salt bridges observed between B5 and $OspC_A$. The two salt bridges formed between B5's V_H domain and $OpsC_A$ involved H2 Glu-54 with $OspC_A$'s Lys-188 and H1 His-32 with Glu-181. The third salt bridge involved V_H framework residue Glu-1 and $OspC_A$ Lys-166 (**Figure 4**). The B5 V_L domain formed five hydrogen bonds (eight hydrogen bonds for the second B5-$OspC_A$ interface within the asymmetric unit) including CDR L2 Thr-52 with $OspC_A$ Lys-79, and CDR L2 Tyr-49 with $OspC_A$ Thr-162. There were no salt bridges between B5 V_L domain and $OspC_A$.

Collectively, the B5 CDR H1, H2, and H3 elements contacted $OspC_A$ α-helix 1 and α-helix 6, along with the loop between α-helices 5 and 6 (loop 5-6). The CDR H3 element also buried 30 $Å^2$ of α-helix 2' in the absence of any H-bonds or salt bridges. CDRs L1, L2, and L3 contacted $OspC_A$ α-helices 1 and 5, β-strands 1 and 2, as well as the loop region immediately N-terminal to α-helix 6. CDR L1 and L3 interacted with α-helix 2', burying 364 $Å^2$ and forming a single H-bond between CDR L1 Asn-30 and Gln-110 in $OspC_A$. The fact that B5 Fabs straddle the OspC dimer interface not only explains conformation-dependent nature of B5's epitope, but more broadly the observation that immunizing mice with homodimeric OspC is more effective than monomeric OspC at eliciting protective antibodies (Edmondson et al., 2017).

Structural basis of B5 IgG specificity for $OspC_A$. To elucidate the structural basis for B5 IgG's specificity for $OspC_A$, we solved the crystal structures of recombinant $OspC_B$ and $OspC_K$ at 1.5 Å and 1.9 Å resolution, respectively, in the $P2_1$ space group (**Figure S4**). $OspC_B$

and $OspC_K$ each formed homodimers nearly identical to $OspC_A$ (unbound or bound to B5). Specifically, $OspC_B$ and $OspC_K$ monomers each consisted of four long α-helices (1, 2, 3, 6), two shorter α–helices (4 and 5) and a two stranded β-sheet (**Figure S4**). The RMSD between the homodimeric $OspC_A$ (bound to B5) versus $OspC_B$ and $OspC_K$ ranged from 0.8 Å to 1.4 Å. In each case, the OspC dimer interface is predominantly hydrophobic, with ~80% of the protein atoms in the interface being nonpolar. The monomeric form of $OspC_A$ (with or without B5 Fab bound) was structurally more similar to $OspC_K$ than $OspC_B$, with an RMSD of ~0.7 Å. A deletion at residue 74 and an insertion of residue 165 in $OspC_B$ relative to $OspC_A$ and $OspC_K$ accounts for its significantly greater structural deviation, as exhibited by an RMSD of 0.9 Å when superposed onto $OspC_A$ or $OspC_K$ monomers. After molecular replacement calculations were performed, the resulting phase information was used to calculate electron density maps utilized to manually insert the correct residues into each model and manually build other regions of each model for the $OspC_B$ and $OspC_K$ structures. Crystallographic and refinement data for each structure demonstrated a refined molecular model with excellent agreement to the crystallographic data, as well as excellent geometry (**Table S1**).

Superpositioning the B5-$OspC_A$ complex onto $OspC_B$ and $OspC_K$ revealed several structural attributes that likely account for B5's inability to recognize $OspC_B$ and $OspC_K$. One prominent feature involves the contact between B5 Trp-100 with Gly-174 in $OspC_A$. In $OspC_B$ and $OspC_K$, Glu-175 is superposed with $OspC_A$ Gly-174. The bulkier glutamic acid (Glu) side chain at position 175 would be expected to sterically clash with Trp-100 (**Figure 5**; **Figure S5**). Specifically, the side chain positions of Trp-100 (B5) and Glu-175 ($OspC_B$, $OspC_K$) are both highly preferred rotamers that would impede a B5 interaction. Furthermore, in the case of $OspC_B$, an "insertion" of Ala-165 within loop 5-6 in $OspC_B$ relative to $OspC_A$ alters the configuration of the loop resulting in a theoretical clash with Tyr-49 of B5 (**Figure 5B**; **Figure S5**). $OspC_B$ is also incapable H-bonding with B5 Tyr-49, due to an Ala rather than a Thr at position 162, as is the case in $OspC_A$. The absence of this H-bond donor would be expected to compromise the B5- $OspC_B$ interaction. Another structural feature in $OspC_B$ disfavoring B5 binding includes deletion of one residue immediately before Lys-74 in $OspC_B$. This deletion substantially altered residue positions 73-75 within α-helix 1 of $OspC_B$ relative to the same residues in $OspC_A$ and $OspC_K$. As a result, the superposed side chain of Lys-74 in $OspC_B$ clashes with B5 Tyr-102. Though several preferred rotamers of $OspC_B$ Lys-74 can readily pivot away

from B5 Tyr-102 alleviating the close encounter between these two residues, movement of Lys-74 away from Tyr-102 and B5 residue Ala-50 would significantly reduce contact between B5 and $OspC_B$ by ~50 $Å^2$ likely diminishing B5 binding to $OspC_B$ (**Figure 5C**; **Figure S5**). In the case of $OspC_K$, divergent primary amino acid sequences at consequential residues certainly contribute to lack of B5 recognition. For example, $OspC_A$ Lys161 forms a π-cation interaction with B5 Trp-100, which cannot occur in the case of $OspC_K$ due to an Ile residue at this position (**Figure 5D**; **Figure S5**). To determine the potential cross-reactivity of B5 with the other OspC types, we looked at the primary sequence conservation across each OspC focusing on regions in $OspC_A$ that support B5 binding while also considering regions in $OspC_B$ and $OspC_K$ that seemingly antagonize B5 interaction. Two two OspC types, C3 and I3, with 76% and 78% overall sequence identities to $OspC_A$, would predictably interact with B5. C3 and I3 possess similar sequences within α-helix 1 and loop 5-6 along with a few other key B5 contact residues found in $OspC_A$ (**Figure S5**). For example, $OspC_{I3}$ is similar to $OspC_A$ in that it has a Gly at position 174, providing ample room to contact B5's Trp-100. In the case of $OspC_{C3}$, an Asp residue replaces Gly-174; while the Asp side chain is larger than Gly there is still sufficient space to engage Trp-100 in B5. It is interesting that Baum and colleagues demonstrated that $OspC_A$ and $OspC_{I3}$ were most immunologically cross-reactive pairs in a protein microarray consisting of 23 OspC types (Baum *et al.*, 2013). Elucidating structural insights into the molecular interactions that promote or repel protective antibodies has important implications for rational vaccine design.

Overlap between B5's footprint and human linear B cell epitopes on OspC. Numerous studies have identified OspC-derived peptides that react with human sera from Lyme disease patients and that have been proposed to have utility of serodiagnosis (**Table 3**). Positioning of seven such linear epitopes on the structure of $OspC_A$ revealed that four of them fall within B5's footprint (**Figure 6**). These results reveal overlap between conformation-dependent and -independent epitopes on the surface of OspC.

Conclusion. OspC is a multifunctional lipoprotein that facilitates both *B. burgdorferi* tick-to-host transmission and infectivity (Caine and Coburn, 2016). OspC is also of interest as a next generation Lyme disease vaccine (Dattwyler and Gomes-Solecki, 2022; Wormser, 2022). Although structures of OspC types A, E, and I were solved two decades ago, the identification of protective B cell epitopes on OspC has been limited to linear (peptide) targets (Arnaboldi et al.,

2013; Earnhart *et al.*, 2005; Norek and Janda, 2017). Thus, the structure reported here between $OspC_A$ and Fabs derived from the mouse MAb, B5, represents the first high-resolution image of a protective B cell epitope on OspC. The B5 Fab-$OspC_A$ complex is stunning in that B5 attacks OspC in a side-on fashion and contacts residues (Asp-70, Glu-71) that form a cavity proposed to serve as binding site for tick- or mammalian-derived ligands (Eicken *et al.*, 2001; Kumaran *et al.*, 2001). The structure also revealed that B5 Fabs straddle the $OspC_A$-$OspC_A$' dimer interface, thereby explaining (at least in part) the conformation-dependent nature of B5's epitope (Gilmore and Mbow, 1999). Ultimately the results of this study advance our understanding of serotype-specific immunity to *B. burgdorferi*, as well as opening avenues for structure-based OspC vaccine development (Ward and Wilson, 2020).

Materials and Methods

Mouse and chimeric B5 IgG MAbs. Lyophilized B5 IgG from CDC was reconstituted to final concentration of 6 mg/ml. B5 Fab fragments were generated by papain digestion followed by affinity depletion of the Fc fragment by Protein A FPLC chromatography. The resulting B5 Fab was purified to homogeneity by size-exclusion chromatography (SEC) using a Superdex 200 16/60 gel filtration column. The B5 mouse hybridoma was cultured as described from frozen aliquot (Mbow *et al.*, 1999). In addition, to ensure sufficient supply of B5 MAb, the mouse B5 V_H and V_L regions were cloned into human IgG1 Fc and κ light chain expression vectors and used to transfect Expi293 cells following protocols previously described (Wang et al., 2016). The resulting chimeric B5 IgG1 was purified and used for dot blot and flow cytometry analysis. Fabs were generated from murine B5 IgG by papain digestion followed by affinity depletion of the Fc fragment by Protein A FPLC chromatography. The resulting B5 Fab was purified to homogeneity by size-exclusion chromatography (SEC) using a Superdex 200 16/60 gel filtration column.

Affinity measurement using biolayer interferometry (BLI). Biotinylated $OspC_A$ (3 µg/mL) in buffer (PBS containing 2% w/v BSA) was captured onto streptavidin biosensors (#18-5019, Sartorius, Goettingen, Germany) for 5 min. After 3 min of baseline in buffer, sensors were then exposed to a 2-fold serial dilution of MAb B5, ranging from 100 to 1.56 nM, for 5 min. The sensors were then dipped into wells containing buffer alone for 30 min. An eighth sensor was also loaded with biotinylated-$OspC_A$, but not exposed to MAb B5, and was thus used as a

background drift control, and subtracted from the other sensor data. The raw sensor data was then loaded into the Data Analysis HT 12.0 software, and the data was fit to a 1:2 bivalent analyte model. Data was captured on an Octet RED96e Biolayer Interferometer (Sartorius) using the Data Acquisition 12.0 software.

Indirect fluorescent antibody staining and flow cytometry. A derivative of *B. burgdorferi* strain B31 over expressing OspC was kindly provided by Dr. Yi-Pin Lin (Wadsworth Center). The strain was cultured in BSK-II media at 37°C with 5% CO_2 to mid-log phase. Cells were collected by centrifugation (3,300 x *g*), washed with PBS, resuspended in BSK-II (minus phenol red indicator) at a final concentration of $1x10^8$ cells/ml, and incubated at room temperature for 30 min. A total of $5x10^6$ cells in 50 µl were incubated with 10 µg/ml of chimeric B5 IgG1 at 37°C for 1 h. Incubation with an isotype control, PB10, was included as a negative control (Rong et al., 2020). The reaction volume was then increased with the addition of 450 µl of BSK-II (minus phenol red), and 2° ab (goat anti-human IgG (H+L)-Alexa 647; Invitrogen) was added at 1/500 dilution and allowed to incubate at 37°C for 30 min. Alexa-647 labeled cells were analyzed on a BD FACS Calibur flow cytometer. Data was obtained and analyzed using BD's CellQuest Pro software.

Dot blot. Recombinant OspC types A, B, and K (**Table 1**) at 0.5 µg/ul, were 5-fold serially diluted in PBS, and 2 µl of each dilution was spotted on a dry nitrocellulose membrane. The spots were allowed to air-dry for 1 h, then blocked with 5% milk in 1x TBS-T for 18 h, and incubated with 0.1 µg/ml chimeric B5 IgG1 in 5% milk 1x TBS-T at room temperature for 1 h. The membrane was then washed twice with 1x TBS-T, incubated with a 1:10,000 dilution goat anti-human IgG (H+L)-HRP (Invitrogen), and washed twice more before detection with ECL (ECL Plus Western Blotting Substrate; Pierce, ThermoFisher, Waltham, MA). Images were acquired and analyzed using an iBright 1500 (Invitrogen).

OspC ELISA. B5 IgG was coated onto wells of a 96 well Immulon 4HBX plate (ThermoFisher, Waltham, MA) at 1 µg/mL in PBS overnight at 4ºC. Wells were then blocked for 2 h at room temperature with 2% goat serum in 0.1% Tween-20 in PBS. Biotinylated OspC Types A, B and K were then diluted 2-fold across the plate, starting at 20 µg/mL. Plates were washed, and then captured biotinylated OspC was detected with avidin-HRP (Pierce, Rockford, IL) for 1 h. Plates were washed again, and capture was visualized with SureBlue TMB

(SeraCare, Milford, MA). The reaction was stopped with 1M phosphoric acid, and the optical density at 450 nm was read using a SpectraMax iD3 (Molecular Devices, San Jose, CA).

LC-MS analysis. For peptic peptide mapping, recombinant $OspC_A$ was diluted with quench solution (200 mM glycine, pH 2.5) and 50 pmol sample was injected in each run. $OspC_A$ was digested by in-house prepared immobilized pepsin column (2.1×50 mm) (Wang et al., 2002). Digested peptides were by trapped and desalted by C-8 (Zorbax 300SB C8, 2.1 x 12.5 mm, 5 µm particles) for 120 s and separated by a C-18 column (Zorbax 300SB 2.1 × 50 mm, 3.5 µm particle diameter, Agilent, Santa Clara, CA). For LC, mobile phase A was 0.1% formic acid in water, and B was 0.1% formic acid in acetonitrile. A total of 25 min LC method, 10 min with 15%-35%B was used to separate peptides and 15 min was used for cleaning purpose. Peptide were detected and mass was measured by quadruple time of flight mass spectrometer Q-TOF mass spectrometer (Agilent 6530 in ESI-positive ion mode). All the peptic peptides were assigned by tandem mass spectrometry (collision induced dissociation (CID) fragmentation). Agilent MassHunter Qualitative Analysis with BioConfirm (version B.07.00) software was used for the analysis of all the mass spectrometry data. A total of 87 peptides were identified and mapped in Fig. S1. This map shows 100% $OspC_A$ sequence coverage with median length 17.0 residues and 8.6 average redundancy.

Hydrogen exchange-mass spectrometry (HX-MS) and data analysis. $OspC_A$ and B5 MAb were buffer exchanged and assayed by our previous protocol (Haque *et al.*, 2022). Previously flash frozen $OspC_A$ (19µM) was thawed at room temperature. B5 sample was collated from 4°C and buffer exchanged on the day of experiment. Free protein state ($OspC_A$) sample was prepared by diluting 19µM $OspC_A$ to 9µM by the addition of 20 mM phosphate, 100 mM NaCl, pH 7.40. Bound state ($OspC_A$ +B5) was prepared by three strokes mixing and adjusted to a final concentration of 9 µM. HX-MS labeling conditions, robot methods, maximally deuterated experiment (OspA paper) protocol, data analysis was done as recently reported (Haque *et al.*, 2022).

Cloning, expression, and purification of OspC. The PCR amplicon encoding *B. burgdorferi* $OspC_A$ (residues 38 to 201) was subcloned into the pSUMO expression vector that contained an N-terminal deca-histidine and SUMO tag. The PCR amplicons for *B. burgdorferi* $OspC_B$ and $OspC_K$ containing residues 38 to 202 were subcloned into the pMCSG7 expression vector that contained an N-terminal deca-histidine tag. Cloning was performed using standard

ligase independent cloning (LIC). All OspC types were expressed in *E. coli* strain BL21 (DE3). The transformed bacteria were grown at 37°C in TB medium and induced at 20°C at an OD_{600} of 0.6 with 0.1 mM IPTG for ~16 h. After induction, cells were harvested and resuspended in 20 mM HEPES [pH 7.5] and 150 mM NaCl. The cell suspension was sonicated and centrifuged at 30,000 x *g* for 30 min. After centrifugation, the protein-containing supernatant was purified by nickel-affinity and size-exclusion chromatography on an AKTAxpress system (GE Healthcare), which consisted of a 1 mL nickel affinity column followed by a Superdex 200 16/60 gel filtration column. The elution buffer consisted of 0.5 M imidazole in binding buffer, and the gel filtration buffer consisted of 20 mM HEPES [pH 7.5], 150 mM NaCl, and 20 mM imidazole. Fractions containing each OspC type were pooled and subject to TEV protease cleavage (1:10 weight ratio) for 3 h at room temperature to remove respective fusion protein tags. The cleaved proteins were passed over a 1mL Ni-NTA agarose (Qiagen) gravity column to remove TEV protease, cleaved residues, and uncleaved fusion protein. After purification, Fab B5 was complexed with $OspC_A$ in a 1:1 stoichiometry, then concentrated to 10 mg/ml final for all crystallization trials.

Crystallization and data collection. All crystals were grown by sitting drop vapor diffusion using a protein to reservoir volume ratio of 1:1 with total drop volumes of 0.2 µl. Crystals of the B5 Fab- $OspC_A$ complex were produced at 22°C using a crystallization solution containing 100 mM sodium cacodylate pH 6.5, 5% PEG 8K, and 40% MPD. Crystals of the $OspC_B$ were produced at 22°C using a crystallization solution containing 100 mM sodium phosphate citrate pH 4.2, 41.9% PEG 600 Crystals of the $OspC_K$ were produced at 4°C using a crystallization solution containing 100 mM Tris pH 8.5, 40% PEG 400, 200 mM LiSO4, 10 mM 2-aminoethanesulfonic acid. All crystals were flash frozen in liquid nitrogen after a short soak in the appropriate crystallization buffers supplemented with 25% ethylene glycol. Data were collected at the 24-ID-E beamline at the Advanced Photon Source, Argonne National Labs. All data was indexed, merged, and scaled using HKL2000 (Otwinowski and Minor, 1997) then converted to structure factor amplitudes using CCP4 (Winn et al., 2011).

Structure determination and refinement. The B5 Fab-$OspC_A$ complex, $OspC_B$, and $OspC_K$ structures were solved by molecular replacement using Phaser (Otwinowski and Minor, 1997). Molecular replacement calculations were performed using the coordinates of the murine monoclonal Fab 3E6 V_H and C_H1 domains (PDB ID: 4KI5) along with the V_L and C_L domains of the human germline antibody hepatitis E virus E2S antibody (PDB ID: 3RKD) as the search

model for Fab B5 in the B5-OspC_A complex. The OspC coordinates (PDB ID: 1GGQ) were used as the search model for OspC_A in the OspC_A-B5 complex. The same OspC coordinates (PDB ID: 1GGQ) were also used as search models for the OspC_B and OspC_K structure determinations. The resulting phase information from molecular replacement was used for some manual model building of each structure solved using the graphics program COOT (Emsley et al., 2010) and structural refinement employing the PHENIX package (Adams et al., 2010). Data collection and refinement statistics are listed in **Table S1**, as are the Protein Data Bank (http://www.rcsb.org/pdb/) codes associated with each of the three structures generated in this study (B5-OspC_A, PDB ID 7UIJ; OspC_B, PDB ID 7UJ2; OspC_K, PDB ID 7UJ6). Molecular graphics were prepared using PyMOL (Schrodinger, DeLano Scientific LLC, Palo Alto, CA).

Acknowledgements

We gratefully acknowledge the Wadsworth Center's Tissue and Cell culture facility for preparing BSK II media, and Dr. Renjie Song in the Immunology Core for assistance with flow cytometry. We thank Dr. Timothy LaRocca (Albany College of Pharmacy and Health Sciences) and Dr. Graham Willsey for insightful discussions and assistance. We thank Elizabeth Cavosie for administrative assistance. This work was supported by the National Institute of Allergy and Infectious Diseases (NIAID), National Institutes of Health, Department of Health and Human Services Contract No. 75N93019C00040. This work is based upon research conducted at the Northeastern Collaborative Access Team beamlines, which are funded by the National Institute of General Medical Sciences from the National Institutes of Health (P30 GM124165). The Eiger 16M detector on the 24-ID-E beam line is funded by a NIH-ORIP HEI grant (S10OD021527).

References Cited

Adams, P.D., Afonine, P.V., Bunkoczi, G., Chen, V.B., Davis, I.W., Echols, N., Headd, J.J., Hung, L.W., Kapral, G.J., Grosse-Kunstleve, R.W., et al. (2010). PHENIX: a comprehensive Python-based system for macromolecular structure solution. Acta Crystallogr D Biol Crystallogr *66*, 213-221. 10.1107/S0907444909052925

S0907444909052925 [pii].

435 Angalakurthi, S.K., Vance, D.J., Rong, Y., Nguyen, C.M.T., Rudolph, M.J., Volkin, D., Middaugh, C.R.,
436 Weis, D.D., and Mantis, N.J. (2018). A Collection of Single-Domain Antibodies that Crowd Ricin
437 Toxin's Active Site. Antibodies (Basel) *7*. 10.3390/antib7040045.
438 Arnaboldi, P.M., Seedarnee, R., Sambir, M., Callister, S.M., Imparato, J.A., and Dattwyler, R.J. (2013).
439 Outer surface protein C peptide derived from Borrelia burgdorferi sensu stricto as a target for
440 serodiagnosis of early lyme disease. Clin Vaccine Immunol *20*, 474-481. 10.1128/CVI.00608-12.
441 Barbour, A.G., and Travinsky, B. (2010). Evolution and distribution of the ospC Gene, a transferable
442 serotype determinant of Borrelia burgdorferi. MBio *1*. 10.1128/mBio.00153-10.
443 Baum, E., Randall, A.Z., Zeller, M., and Barbour, A.G. (2013). Inferring epitopes of a polymorphic
444 antigen amidst broadly cross-reactive antibodies using protein microarrays: a study of OspC proteins
445 of Borrelia burgdorferi. PLoS One *8*, e67445. 10.1371/journal.pone.0067445.
446 Bhatia, B., Hillman, C., Carracoi, V., Cheff, B.N., Tilly, K., and Rosa, P.A. (2018). Infection history of
447 the blood-meal host dictates pathogenic potential of the Lyme disease spirochete within the feeding
448 tick vector. PLoS Pathog *14*, e1006959. 10.1371/journal.ppat.1006959.
449 Bockenstedt, L.K., Hodzic, E., Feng, S., Bourrel, K.W., de Silva, A., Montgomery, R.R., Fikrig, E.,
450 Radolf, J.D., and Barthold, S.W. (1997). Borrelia burgdorferi strain-specific Osp C-mediated
451 immunity in mice. Infect Immun *65*, 4661-4667. 10.1128/iai.65.11.4661-4667.1997.
452 Brier, S., Rasetti-Escargueil, C., Wijkhuisen, A., Simon, S., Marechal, M., Lemichez, E., and Popoff,
453 M.R. (2021). Characterization of a highly neutralizing single monoclonal antibody to botulinum
454 neurotoxin type A. FASEB J *35*, e21540. 10.1096/fj.202002492R.
455 Buckles, E.L., Earnhart, C.G., and Marconi, R.T. (2006). Analysis of antibody response in humans to the
456 type A OspC loop 5 domain and assessment of the potential utility of the loop 5 epitope in Lyme
457 disease vaccine development. Clin Vaccine Immunol *13*, 1162-1165. 10.1128/CVI.00099-06.
458 Bunikis, J., Garpmo, U., Tsao, J., Berglund, J., Fish, D., and Barbour, A.G. (2004). Sequence typing
459 reveals extensive strain diversity of the Lyme borreliosis agents Borrelia burgdorferi in North
460 America and Borrelia afzelii in Europe. Microbiology (Reading) *150*, 1741-1755.
461 10.1099/mic.0.26944-0.
462 Caimano, M.J., Groshong, A.M., Belperron, A., Mao, J., Hawley, K.L., Luthra, A., Graham, D.E.,
463 Earnhart, C.G., Marconi, R.T., Bockenstedt, L.K., et al. (2019). The RpoS Gatekeeper in Borrelia
464 burgdorferi: An Invariant Regulatory Scheme That Promotes Spirochete Persistence in Reservoir
465 Hosts and Niche Diversity. Front Microbiol *10*, 1923. 10.3389/fmicb.2019.01923.
466 Caine, J.A., and Coburn, J. (2016). Multifunctional and Redundant Roles of Borrelia burgdorferi Outer
467 Surface Proteins in Tissue Adhesion, Colonization, and Complement Evasion. Front Immunol *7*, 442.
468 10.3389/fimmu.2016.00442.

469 Chen, G., Karauzum, H., Long, H., Carranza, D., Holtsberg, F.W., Howell, K.A., Abaandou, L., Zhang,
470 B., Jarvik, N., Ye, W., et al. (2019). Potent Neutralization of Staphylococcal Enterotoxin B In Vivo
471 by Antibodies that Block Binding to the T-Cell Receptor. J Mol Biol *431*, 4354-4367.
472 10.1016/j.jmb.2019.03.017.
473 Dattwyler, R.J., and Gomes-Solecki, M. (2022). The year that shaped the outcome of the OspA vaccine
474 for human Lyme disease. NPJ Vaccines *7*, 10. 10.1038/s41541-022-00429-5.
475 De Silva, A.M., and Fikrig, E. (1995). Growth and migration of Borrelia burgdorferi in Ixodes ticks
476 during blood feeding. Am J Trop Med Hyg *53*, 397-404. 10.4269/ajtmh.1995.53.397.
477 Di, L., Akther, S., Bezrucenkovas, E., Ivanova, L., Sulkow, B., Wu, B., Mneimneh, S., Gomes-Solecki,
478 M., and Qiu, W.G. (2022). Maximum antigen diversification in a lyme bacterial population and
479 evolutionary strategies to overcome pathogen diversity. ISME J *16*, 447-464. 10.1038/s41396-021-
480 01089-4.
481 Earnhart, C.G., Buckles, E.L., Dumler, J.S., and Marconi, R.T. (2005). Demonstration of OspC type
482 diversity in invasive human lyme disease isolates and identification of previously uncharacterized
483 epitopes that define the specificity of the OspC murine antibody response. Infect Immun *73*, 7869-
484 7877. 10.1128/IAI.73.12.7869-7877.2005.
485 Earnhart, C.G., Leblanc, D.V., Alix, K.E., Desrosiers, D.C., Radolf, J.D., and Marconi, R.T. (2010).
486 Identification of residues within ligand-binding domain 1 (LBD1) of the Borrelia burgdorferi OspC
487 protein required for function in the mammalian environment. Mol Microbiol *76*, 393-408.
488 10.1111/j.1365-2958.2010.07103.x.
489 Earnhart, C.G., and Marconi, R.T. (2007). OspC phylogenetic analyses support the feasibility of a
490 broadly protective polyvalent chimeric Lyme disease vaccine. Clin Vaccine Immunol *14*, 628-634.
491 10.1128/CVI.00409-06.
492 Edmondson, D.G., Prabhakaran, S., Norris, S.J., Ullmann, A.J., Piesman, J., Dolan, M., Probst, C.,
493 Radzimski, C., Stöcker, W., and Komorowski, L. (2017). Enhanced Protective Immunogenicity of
494 Homodimeric Borrelia burgdorferi Outer Surface Protein C. Clin Vaccine Immunol *24*.
495 10.1128/cvi.00306-16.
496 Eicken, C., Sharma, V., Klabunde, T., Lawrenz, M.B., Hardham, J.M., Norris, S.J., and Sacchettini, J.C.
497 (2002). Crystal structure of Lyme disease variable surface antigen VlsE of Borrelia burgdorferi. J
498 Biol Chem *277*, 21691-21696. 10.1074/jbc.M201547200.
499 Eicken, C., Sharma, V., Klabunde, T., Owens, R.T., Pikas, D.S., Hook, M., and Sacchettini, J.C. (2001).
500 Crystal structure of Lyme disease antigen outer surface protein C from Borrelia burgdorferi. J Biol
501 Chem *276*, 10010-10015. 10.1074/jbc.M010062200.

Emsley, P., Lohkamp, B., Scott, W.G., and Cowtan, K. (2010). Features and development of Coot. Acta Crystallogr D Biol Crystallogr *66*, 486-501. 10.1107/S0907444910007493

S0907444910007493 [pii].

Gilmore, R.D., Jr., Kappel, K.J., Dolan, M.C., Burkot, T.R., and Johnson, B.J. (1996). Outer surface protein C (OspC), but not P39, is a protective immunogen against a tick-transmitted Borrelia burgdorferi challenge: evidence for a conformational protective epitope in OspC. Infect Immun *64*, 2234-2239. 10.1128/iai.64.6.2234-2239.1996.

Gilmore, R.D., Jr., and Mbow, M.L. (1999). Conformational nature of the Borrelia burgdorferi B31 outer surface protein C protective epitope. Infect Immun *67*, 5463-5469. 10.1128/IAI.67.10.5463-5469.1999.

Gilmore, R.D., Jr., and Piesman, J. (2000). Inhibition of Borrelia burgdorferi migration from the midgut to the salivary glands following feeding by ticks on OspC-immunized mice. Infect Immun *68*, 411-414. 10.1128/IAI.68.1.411-414.2000.

Gomes-Solecki, M., Arnaboldi, P.M., Backenson, P.B., Benach, J.L., Cooper, C.L., Dattwyler, R.J., Diuk-Wasser, M., Fikrig, E., Hovius, J.W., Laegreid, W., et al. (2020). Protective Immunity and New Vaccines for Lyme Disease. Clin Infect Dis *70*, 1768-1773. 10.1093/cid/ciz872.

Grauslund, L.R., Calvaresi, V., Pansegrau, W., Norais, N., and Rand, K.D. (2021). Epitope and Paratope Mapping by HDX-MS Combined with SPR Elucidates the Difference in Bactericidal Activity of Two Anti-NadA Monoclonal Antibodies. J Am Soc Mass Spectrom *32*, 1575-1582. 10.1021/jasms.0c00431.

Hanincova, K., Mukherjee, P., Ogden, N.H., Margos, G., Wormser, G.P., Reed, K.D., Meece, J.K., Vandermause, M.F., and Schwartz, I. (2013). Multilocus sequence typing of Borrelia burgdorferi suggests existence of lineages with differential pathogenic properties in humans. PLoS One *8*, e73066. 10.1371/journal.pone.0073066.

Haque, H.M.E., Ejemel, M., Vance, D.J., Willsey, G., Rudolph, M.J., Cavacini, L.A., Wang, Y., Mantis, N.J., and Weis, D.D. (2022). Human B Cell Epitope Map of the Lyme Disease Vaccine Antigen, OspA. ACS Infect Dis. 10.1021/acsinfecdis.2c00346.

Hodge, E.A., Naika, G.S., Kephart, S.M., Nguyen, A., Zhu, R., Benhaim, M.A., Guo, W., Moore, J.P., Hu, S.L., Sanders, R.W., and Lee, K.K. (2022). Structural dynamics reveal isolate-specific differences at neutralization epitopes on HIV Env. iScience *25*, 104449. 10.1016/j.isci.2022.104449.

Izac, J.R., Camire, A.C., Earnhart, C.G., Embers, M.E., Funk, R.A., Breitschwerdt, E.B., and Marconi, R.T. (2019). Analysis of the antigenic determinants of the OspC protein of the Lyme disease spirochetes: Evidence that the C10 motif is not immunodominant or required to elicit bactericidal antibody responses. Vaccine *37*, 2401-2407. 10.1016/j.vaccine.2019.02.007.

536 Izac, J.R., and Marconi, R.T. (2019). Diversity of the Lyme Disease Spirochetes and its Influence on
537 Immune Responses to Infection and Vaccination. Vet Clin North Am Small Anim Pract *49*, 671-686.
538 10.1016/j.cvsm.2019.02.007.
539 Izac, J.R., O'Bier, N.S., Oliver, L.D., Jr., Camire, A.C., Earnhart, C.G., LeBlanc Rhodes, D.V., Young,
540 B.F., Parnham, S.R., Davies, C., and Marconi, R.T. (2020). Development and optimization of OspC
541 chimeritope vaccinogens for Lyme disease. Vaccine *38*, 1915-1924. 10.1016/j.vaccine.2020.01.027.
542 Kugeler, K.J., Schwartz, A.M., Delorey, M.J., Mead, P.S., and Hinckley, A.F. (2021). Estimating the
543 Frequency of Lyme Disease Diagnoses, United States, 2010-2018. Emerg Infect Dis *27*, 616-619.
544 10.3201/eid2702.202731.
545 Kumaran, D., Eswaramoorthy, S., Luft, B.J., Koide, S., Dunn, J.J., Lawson, C.L., and Swaminathan, S.
546 (2001). Crystal structure of outer surface protein C (OspC) from the Lyme disease spirochete,
547 Borrelia burgdorferi. EMBO J *20*, 971-978. 10.1093/emboj/20.5.971.
548 Malito, E., Faleri, A., Lo Surdo, P., Veggi, D., Maruggi, G., Grassi, E., Cartocci, E., Bertoldi, I.,
549 Genovese, A., Santini, L., et al. (2013). Defining a protective epitope on factor H binding protein, a
550 key meningococcal virulence factor and vaccine antigen. Proc Natl Acad Sci U S A *110*, 3304-3309.
551 10.1073/pnas.1222845110

552 1222845110 [pii].
553 Mathiesen, M.J., Holm, A., Christiansen, M., Blom, J., Hansen, K., Ostergaard, S., and Theisen, M.
554 (1998). The dominant epitope of Borrelia garinii outer surface protein C recognized by sera from
555 patients with neuroborreliosis has a surface-exposed conserved structural motif. Infect Immun *66*,
556 4073-4079. 10.1128/IAI.66.9.4073-4079.1998.
557 Mbow, M.L., Gilmore, R.D., Jr., Stevenson, B., Golde, W.T., Piesman, J., and Johnson, B.J. (2002).
558 Borrelia burgdorferi-specific monoclonal antibodies derived from mice primed with Lyme disease
559 spirochete-infected Ixodes scapularis ticks. Hybrid Hybridomics *21*, 179-182.
560 10.1089/153685902760173890.
561 Mbow, M.L., Gilmore, R.D., Jr., and Titus, R.G. (1999). An OspC-specific monoclonal antibody
562 passively protects mice from tick-transmitted infection by Borrelia burgdorferi B31. Infect Immun *67*,
563 5470-5472. 10.1128/IAI.67.10.5470-5472.1999.
564 Nadelman, R.B., Hanincova, K., Mukherjee, P., Liveris, D., Nowakowski, J., McKenna, D., Brisson, D.,
565 Cooper, D., Bittker, S., Madison, G., et al. (2012). Differentiation of reinfection from relapse in
566 recurrent Lyme disease. N Engl J Med *367*, 1883-1890. 10.1056/NEJMoa1114362.
567 Norek, A., and Janda, L. (2017). Epitope mapping of Borrelia burgdorferi OspC protein in homodimeric
568 fold. Protein Sci *26*, 796-806. 10.1002/pro.3125.

569 Ohnishi, J., Piesman, J., and de Silva, A.M. (2001). Antigenic and genetic heterogeneity of Borrelia
570 burgdorferi populations transmitted by ticks. Proc Natl Acad Sci U S A *98*, 670-675.
571 10.1073/pnas.98.2.670.
572 Otwinowski, Z., and Minor, W. (1997). Processing of x-ray diffraction data collected in oscillation
573 mode. . Methods in Enzymology *276*, 307-326.
574 Pal, U., Yang, X., Chen, M., Bockenstedt, L.K., Anderson, J.F., Flavell, R.A., Norgard, M.V., and
575 Fikrig, E. (2004). OspC facilitates Borrelia burgdorferi invasion of Ixodes scapularis salivary glands.
576 J Clin Invest *113*, 220-230. 10.1172/JCI19894.
577 Preac-Mursic, V., Wilske, B., Patsouris, E., Jauris, S., Will, G., Soutschek, E., Rainhardt, S., Lehnert, G.,
578 Klockmann, U., and Mehraein, P. (1992). Active immunization with pC protein of Borrelia
579 burgdorferi protects gerbils against B. burgdorferi infection. Infection *20*, 342-349.
580 10.1007/BF01710681.
581 Probert, W.S., and LeFebvre, R.B. (1994). Protection of C3H/HeN mice from challenge with Borrelia
582 burgdorferi through active immunization with OspA, OspB, or OspC, but not with OspD or the 83-
583 kilodalton antigen. Infect Immun *62*, 1920-1926. 10.1128/iai.62.5.1920-1926.1994.
584 Pulzova, L., Flachbartova, Z., Bencurova, E., Potocnakova, L., Comor, L., Schreterova, E., and Bhide,
585 M. (2016). Identification of B-cell epitopes of Borrelia burgdorferi outer surface protein C by
586 screening a phage-displayed gene fragment library. Microbiol Immunol *60*, 669-677. 10.1111/1348-
587 0421.12438.
588 Radolf, J.D., Strle, K., Lemieux, J.E., and Strle, F. (2021). Lyme Disease in Humans. Curr Issues Mol
589 Biol *42*, 333-384. 10.21775/cimb.042.333.
590 Rana, V.S., Kitsou, C., Dumler, J.S., and Pal, U. (2022). Immune evasion strategies of major tick-
591 transmitted bacterial pathogens. Trends Microbiol. 10.1016/j.tim.2022.08.002.
592 Rong, Y., Torres-Velez, F.J., Ehrbar, D., Doering, J., Song, R., and Mantis, N.J. (2020). An intranasally
593 administered monoclonal antibody cocktail abrogates ricin toxin-induced pulmonary tissue damage
594 and inflammation. Hum Vaccin Immunother *16*, 793-807. 10.1080/21645515.2019.1664243.
595 Rousselle, J.C., Callister, S.M., Schell, R.F., Lovrich, S.D., Jobe, D.A., Marks, J.A., and Wieneke, C.A.
596 (1998). Borreliacidal antibody production against outer surface protein C of Borrelia burgdorferi. J
597 Infect Dis *178*, 733-741.
598 Schwan, T.G., Piesman, J., Golde, W.T., Dolan, M.C., and Rosa, P.A. (1995). Induction of an outer
599 surface protein on Borrelia burgdorferi during tick feeding. Proc Natl Acad Sci U S A *92*, 2909-2913.
600 10.1073/pnas.92.7.2909.

601 Seinost, G., Dykhuizen, D.E., Dattwyler, R.J., Golde, W.T., Dunn, J.J., Wang, I.N., Wormser, G.P.,
602 Schriefer, M.E., and Luft, B.J. (1999). Four clones of Borrelia burgdorferi sensu stricto cause
603 invasive infection in humans. Infect Immun *67*, 3518-3524.
604 Seow, J., Khan, H., Rosa, A., Calvaresi, V., Graham, C., Pickering, S., Pye, V.E., Cronin, N.B.,
605 Huettner, I., Malim, M.H., et al. (2022). A neutralizing epitope on the SD1 domain of SARS-CoV-2
606 spike targeted following infection and vaccination. Cell Rep *40*, 111276.
607 10.1016/j.celrep.2022.111276.
608 Steere, A.C., Strle, F., Wormser, G.P., Hu, L.T., Branda, J.A., Hovius, J.W., Li, X., and Mead, P.S.
609 (2016). Lyme borreliosis. Nat Rev Dis Primers *2*, 16090. 10.1038/nrdp.2016.90.
610 Vinciauskaite, V., and Masson, G.R. (2022). Fundamentals of HDX-MS. Essays Biochem.
611 10.1042/EBC20220111.
612 Wang, I.N., Dykhuizen, D.E., Qiu, W., Dunn, J.J., Bosler, E.M., and Luft, B.J. (1999). Genetic diversity
613 of ospC in a local population of Borrelia burgdorferi sensu stricto. Genetics *151*, 15-30.
614 10.1093/genetics/151.1.15.
615 Wang, L., Pan, H., and Smith, D.L. (2002). Hydrogen exchange-mass spectrometry: optimization of
616 digestion conditions. Mol Cell Proteomics *1*, 132-138.
617 Wang, Y., Kern, A., Boatright, N.K., Schiller, Z.A., Sadowski, A., Ejemel, M., Souders, C.A., Reimann,
618 K.A., Hu, L., Thomas, W.D., Jr., and Klempner, M.S. (2016). Pre-exposure Prophylaxis With OspA-
619 Specific Human Monoclonal Antibodies Protects Mice Against Tick Transmission of Lyme Disease
620 Spirochetes. J Infect Dis *214*, 205-211. 10.1093/infdis/jiw151.
621 Ward, A.B., and Wilson, I.A. (2020). Innovations in structure-based antigen design and immune
622 monitoring for next generation vaccines. Curr Opin Immunol *65*, 50-56. 10.1016/j.coi.2020.03.013.
623 Wilske, B., Luft, B., Schubach, W.H., Zumstein, G., Jauris, S., Preac-Mursic, V., and Kramer, M.D.
624 (1992). Molecular analysis of the outer surface protein A (OspA) of Borrelia burgdorferi for
625 conserved and variable antibody binding domains. Med Microbiol Immunol *181*, 191-207.
626 10.1007/bf00215765.
627 Winn, M.D., Ballard, C.C., Cowtan, K.D., Dodson, E.J., Emsley, P., Evans, P.R., Keegan, R.M.,
628 Krissinel, E.B., Leslie, A.G., McCoy, A., et al. (2011). Overview of the CCP4 suite and current
629 developments. Acta Crystallogr D Biol Crystallogr *67*, 235-242. 10.1107/S0907444910045749
630 S0907444910045749 [pii].
631 Wormser, G.P. (2022). A brief history of OspA vaccines including their impact on diagnostic testing for
632 Lyme disease. Diagn Microbiol Infect Dis *102*, 115572. 10.1016/j.diagmicrobio.2021.115572.

Yu, Z., Carter, J.M., Sigal, L.H., and Stein, S. (1996). Multi-well ELISA based on independent peptide antigens for antibody capture. Application to Lyme disease serodiagnosis. J Immunol Methods *198*, 25-33.

Zhong, W., Stehle, T., Museteanu, C., Siebers, A., Gern, L., Kramer, M., Wallich, R., and Simon, M.M. (1997). Therapeutic passive vaccination against chronic Lyme disease in mice. Proc Natl Acad Sci U S A *94*, 12533-12538. 10.1073/pnas.94.23.12533.

Zuckert, W.R., Kerentseva, T.A., Lawson, C.L., and Barbour, A.G. (2001). Structural conservation of neurotropism-associated VspA within the variable Borrelia Vsp-OspC lipoprotein family. J Biol Chem *276*, 457-463. 10.1074/jbc.M008449200.

Figure Legends

Figure 1. Reactivity of B5 IgG with native and recombinant OspC. (**A, B**). Mid-log phase *B. burgdorferi* over expressing $OspC_A$ was incubated with chimeric B5 IgG or an isotype control (PB10) for 1 h at 37°C, washed and then labeled with Alexa 647-labeled goat anti-human secondary antibody. Cells were analyzed using a BD FACS Calibur flow cytometer. Panel A shows a representative histogram of PB10 (left) and B5 (right) with relative fluorescence plotted on x-axis and number of events plotted on y-axis. In panel B, the total number of Alexa-positive cells following PB10 and B5 treatment from three independent replicates. Asterisks indicate statistical differences ($p < 0.001$) based on Student's t-test. (**C**) Capture of biotin-tagged recombinant OspC types A, B and K by immobilized B5 IgG, as described in Material and Methods. The capture ELISA is representative of three independent replicates. (**D**) Reactivity of B5 IgG with 5-fold serial dilutions of recombinant OspC types A, B and K spotted onto nitrocellulose membrane. Recombinant OspA (rOspA) and PBS were spotted as negative controls.

Figure 2. Localization of B5 IgG binding sites on $OspC_A$ by HX-MS. (**A**) Time-averaged, normalized HX differences ($\Delta\overline{HX}$) between $OspC_A$ and $OspC_A$ bound to B5 IgG. Negative bars denote slower HX in the presence of B5 IgG. The peptide index organizes the peptides from N- to C-terminus. The values are color-coded based on k-means clustering. Extreme cluster values (e.g. –2) denotes stronger effects; (**B**) Peptide resolution map of the B5 IgG epitope showing clustered HX; (**C**) Cartoon (left) and surface (right) representations of $OspC_A$ [PDB ID 1GGQ]

with relative effects of B5 IgG as interpreted from panels A and B. The dark blue shading represents strongly protected regions of $OspC_A$, light blue represents weak (but significant) protection, and black denotes lack of coverage.

Figure 3. Structure of B5 Fab-$OspC_A$. (A) Side-on and (B) top-down ribbon diagrams of $OspC_A$ homodimer ($OspC_A$, $OspC_A$') in complex with B5 Fabs (B5, B5'). The $OspC_A$ is colored in yellow and $OspC_A$' in magenta. The B5 Fab V_H and C_H1 elements are colored light green and the V_L and C_L cyan. The B5' Fab V_H and C_H1 elements are colored in salmon red and V_L and C_L in light gray. The N- and C-termini of $OspC_A$ and $OspC_A$' are labelled accordingly (N, C).

Figure 4. Detailed interactions between B5 and $OspC_A$ revealed from the co-crystal structure. (**A**) Ribbon structure (top-down view) of $OspC_A$ homodimer ($OspC_A$, magenta; $OspC_A$', yellow) in complex with a single B5 Fab (V_H and C_H1 elements, salmon red; V_L and C_L, light gray). The $OspC_A$ residues that engage with B5 are colored blue. Key secondary structures are labeled (α-helices 1, 2, 5, and 6; β-strands 1 and 2); (**B**) Ribbon (left) and surface (right) depiction of an $OspC_A$ homodimer ($OspC_A$, magenta; $OspC_A$', yellow) with B5 interacting residues shaded in dark blue. $OspC_A$ N and C-termini are labelled N and C, respectively. Representations of key (**C**) H-bonds (red dashes) and (**D**) salt bridges (yellow dashes) between $OspC_A$ (magenta) and Fab B5 (salmon red in panel C; gray in panel D). Side chains are drawn as sticks and color coordinated to the main chain color, with nitrogen atoms shaded blue and oxygen atoms shaded red. CDR elements are labelled per convention: CDR-L1, -L2, -L3; CDR-H1, -H2, -H3.

Figure 5. Structural basis of B5 specificity for $OspC_A$. Interface between B5 Fab and $OspC_A$ superposed with $OspC_B$ and $OspC_K$, highlighting interactions that are conceivably disrupted by sequence deviations among OspC types. (**A**) The C-α traces of $OspC_A$ (magenta) bound to B5 (salmon red) with superposed $OspC_B$ (light gray) and $OspC_K$ (dark gray) highlighting potential steric clash between Glu-175 of $OspC_B$ and $OspC_K$ with Trp-100 of B5 Fab. (**B**) C-α traces of $OspC_A$ (magenta) bound to B5 (salmon red) superposed with $OspC_B$ (light gray). The image highlights likely repulsion between Ala-162 of $OspC_B$ with Tyr-49 of B5 Fab. (**C**) C-α traces of $OspC_A$ (magenta) bound to B5 with CDR-H3 (gray) and CDR-L2 (gray) superposed with $OspC_K$

(light gray). The image highlights a potential clash between Lys-74 of $OspC_K$ and B5's Tyr-102. (**D**) The C-α trace of $OspC_A$ (magenta) bound to B5 (salmon red) superposed with $OspC_K$ (dark gray). Ile-162 in $OspC_K$ precludes a potential π-cation interaction that occurs between $OspC_A$ Lys-161 and Trp-100 in B5 Fab. Side chains are drawn as sticks and color coordinated to the main chain color, with nitrogen atoms shaded blue and oxygen atoms shaded red.

Figure 6. Depiction of overlap between linear human B cell epitopes and B5 contact points on OspC. Surface representation of a $OspC_A$ homodimer [shaded gray; PDB ID 1GGQ] with (**A**) B5 contact points (salmon red) from **Figure 3** and (**B**) the location of seven (1-7) previously reported linear B cell epitopes on OspC and reported in **Table 3**. The asterisks (*) indicate proposed overlap with B5 contact points.

TABLES

Table 1. OspC crystal structures and PDB codes

Type	Strain	PDB ID	Reference
A	B31	1GGQ	(Kumaran *et al.*, 2001)
B	ZS7	7UJ2	this study
E	N40	1G5Z	(Eicken et al., 2002)
I	HB19	1F1M	(Kumaran *et al.*, 2001)
K	297	7UJ6	this study

Table 2. Summary of $OspC_A$-B5 binding data and interface information

interface	H-bonds [a]	salt bridges	shape comp. [b]	BSA (Å^2)
1º	9	3	0.68	2040
2º [c]	12	3	0.61	2002

[a], Hydrogen bonds; [b], Shape complementarity score; [c], second RTA-V_HH complex in crystallographic asymmetric unit

Table 3. Human linear B cell epitopes on OspC and putative overlap with B5 contact points

#	Residues[a]	Sequence	B5[b]	IEDB ID[c]	Ref
1	38-53	KGPNLVEISKKITDSN	-	559957	(Pulzova et al., 2016)
2	71-86	EIAAKAIGKKIHQNNG	+	12383	(Yu et al., 1996)
3	104-118	ISTLIKQKLDGLKNE	+	28749	(Yu *et al.*, 1996)
4	130-150	CSETFTNKLKEKHTDLGKEGV	-	6984	(Buckles et al., 2006)
5	156-171	AKKAILITDAAKDKG	+	181187	(Arnaboldi *et al.*, 2013)
6	184-190	LKAAKEM	+	560173	(Pulzova *et al.*, 2016)
7	195-210[b]	PVVAESPKKP	-	49993	(Mathiesen et al., 1998)

[a], sequences from OspC type A (strain B31), except 5 from $OspC_K$; [b], "+" refers to spatial overlap with B5's epitope; [c], refers to the Immune Epitope Database (IEDB).

722

Figure 1

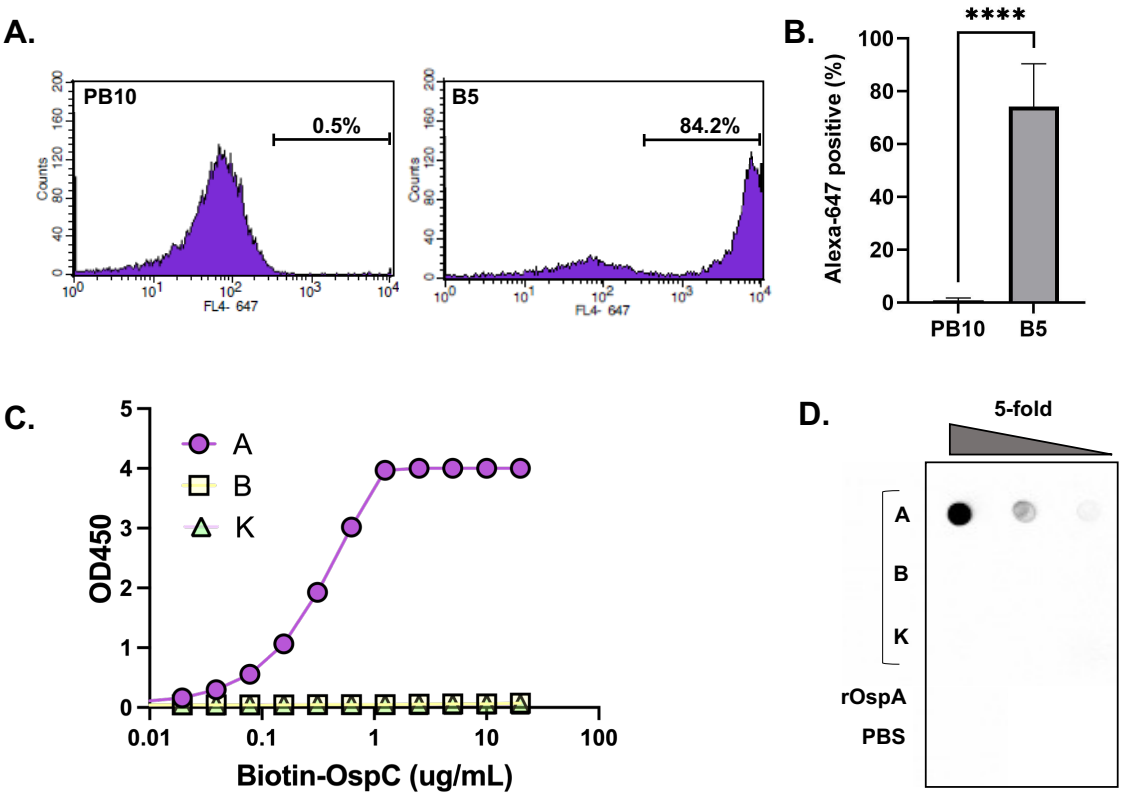
A.
PB10
0.5%
B5
84.2%
Counts
FL4- 647
B.
****
Alexa-647 positive (%)
PB10
B5
C.
A
B
K
OD450
Biotin-OspC (ug/mL)
D.
5-fold
A
B
K
rOspA
PBS

Figure 2

A.

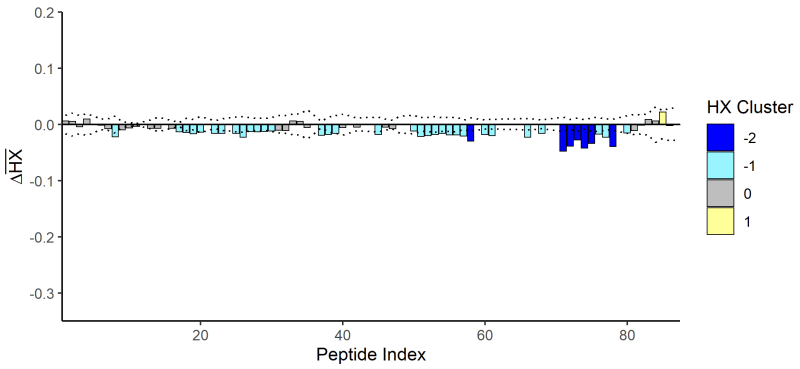
0.2
0.1
0.0
-0.1
-0.2
-0.3
ΔHX
20
40
60
80
Peptide Index
HX Cluster
-2
-1
0
1

B.

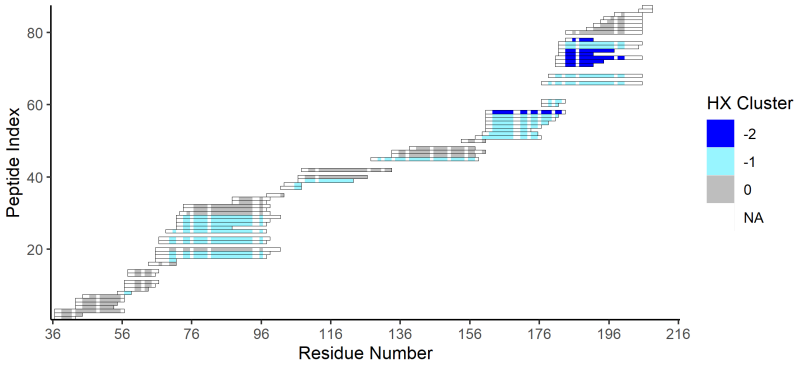
80
60
40
20
Peptide Index
36
56
76
96
116
136
156
176
196
216
Residue Number
HX Cluster
-2
-1
0
NA

C.

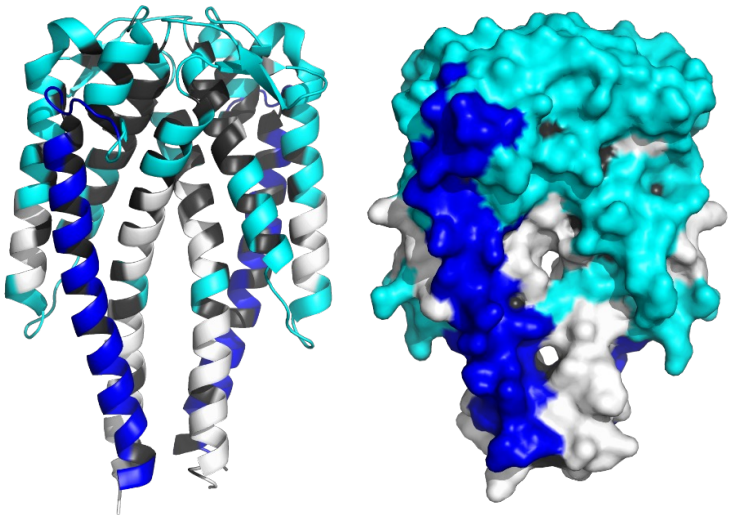

Figure 3

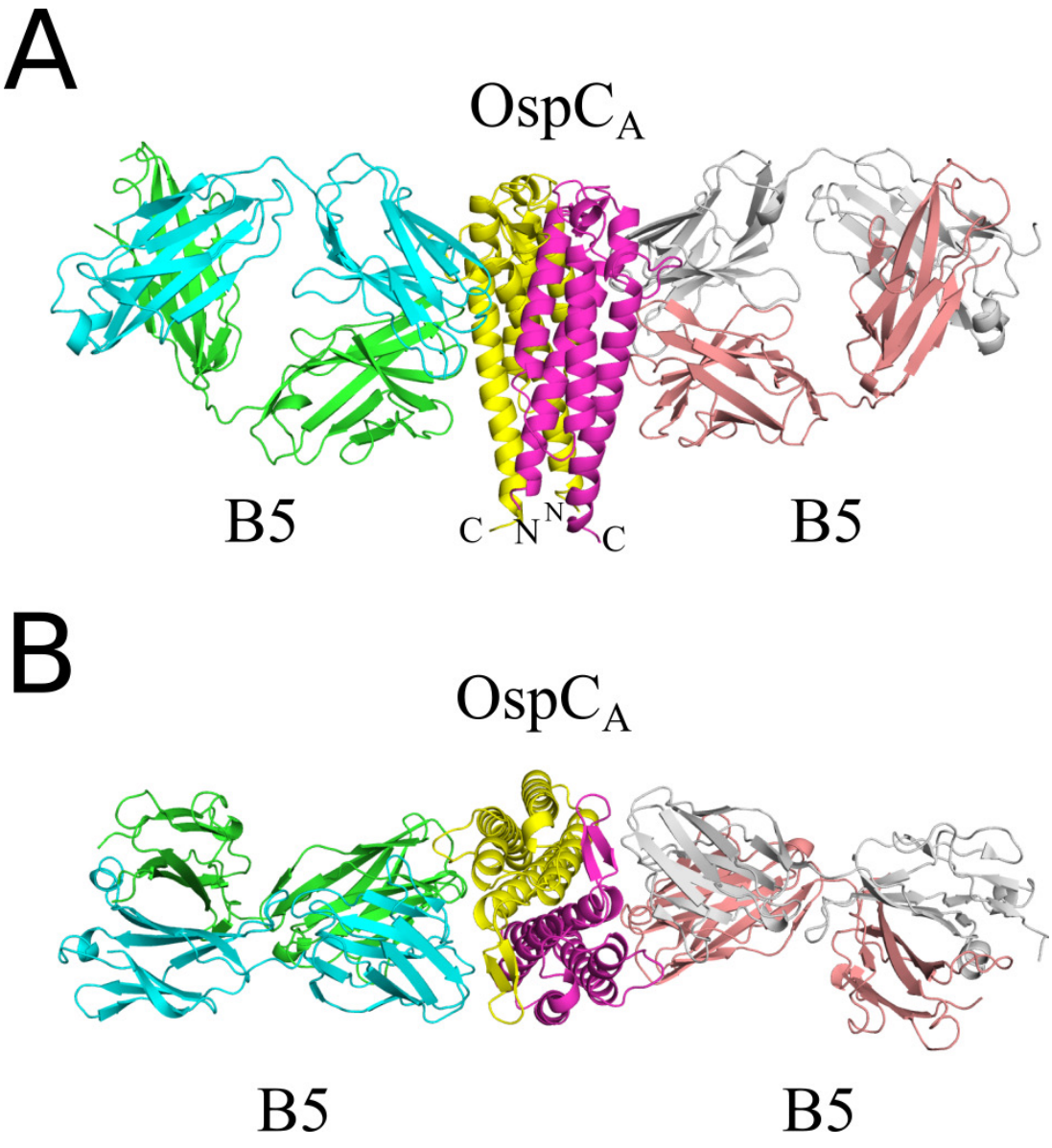

Figure 4

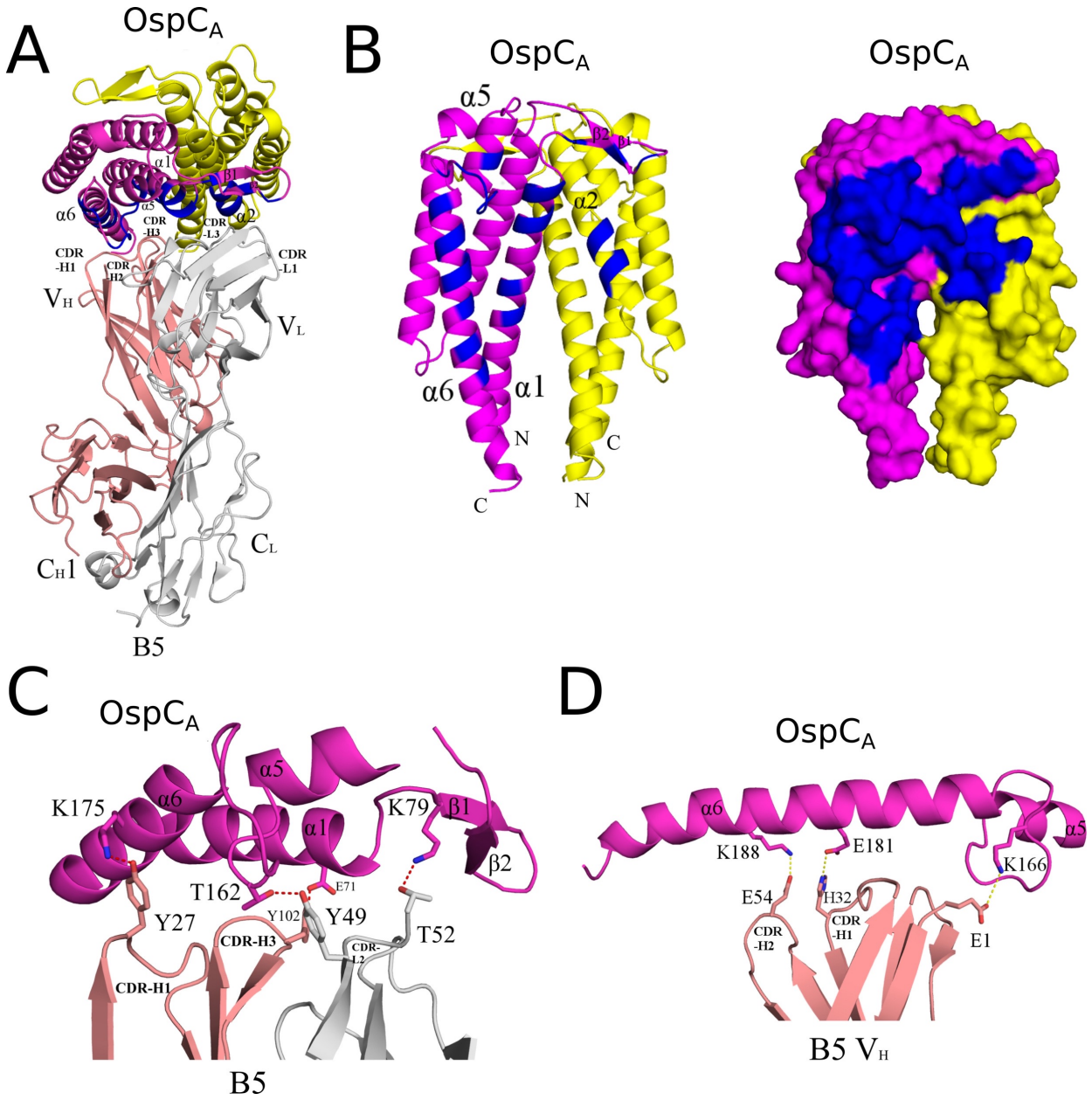
A
OspC$_A$
α1
β1
α5
α6
CDR -H3
CDR -L3
α2
CDR -H1
CDR -H2
CDR -L1
V_H
V_L
C_L
C_H1
B5
B
OspC$_A$
α5
β2
β1
α2
α6
α1
N
C
C
N
OspC$_A$
C
OspC$_A$
α5
K175
α6
α1
K79
β1
β2
T162
E71
Y27
Y102
Y49
T52
CDR-H3
CDR-L2
CDR-H1
B5
D
OspC$_A$
α6
α5
K188
E181
K166
E54
H32
CDR -H2
CDR -H1
E1
B5 V_H

Figure 5

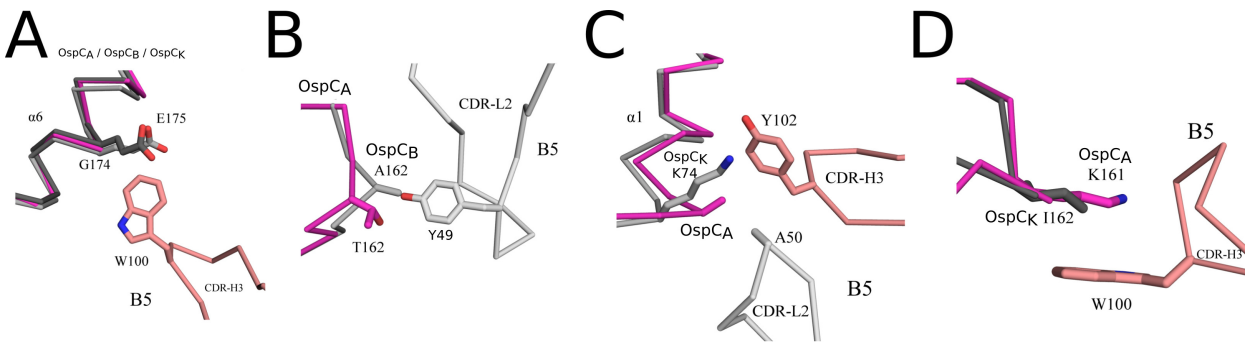
A
OspC$_A$ / OspC$_B$ / OspC$_K$
α6
E175
G174
W100
B5
CDR-H3
B
OspC$_A$
CDR-L2
OspC$_B$
A162
B5
T162
Y49
C
α1
OspC$_K$
K74
Y102
CDR-H3
OspC$_A$
A50
B5
CDR-L2
D
B5
OspC$_A$
K161
OspC$_K$ I162
CDR-H3
W100

Figure 6

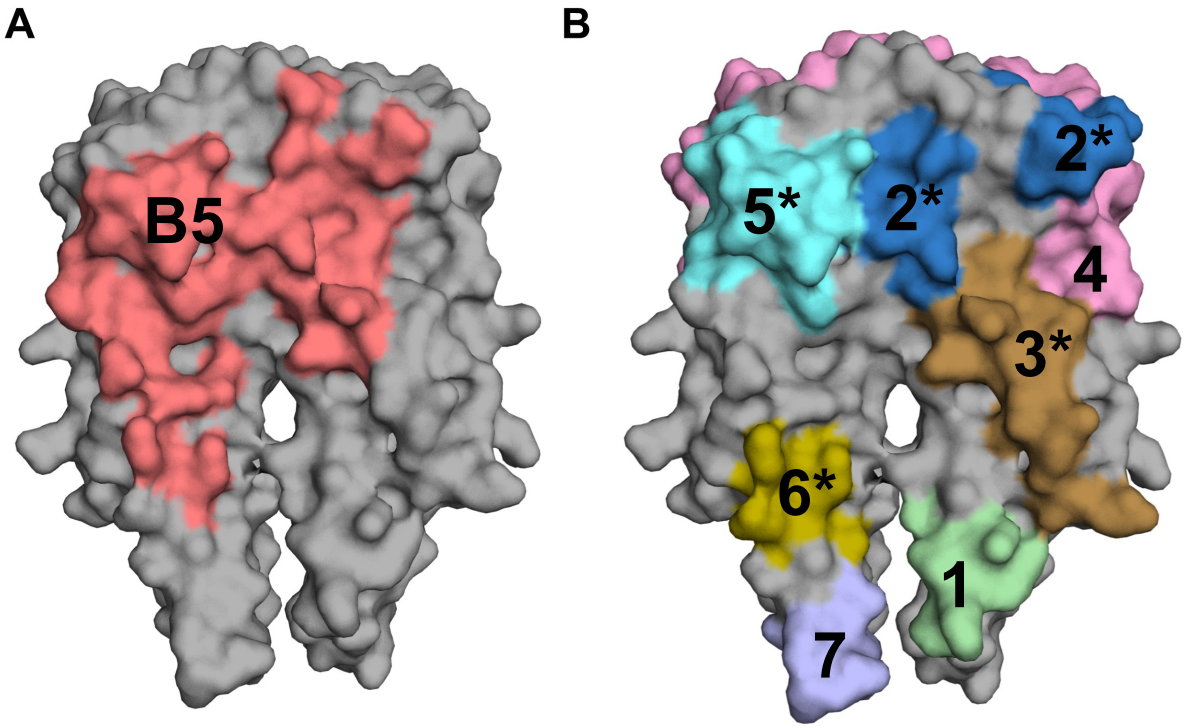

Table S1. Data associated with crystal structures reported in this study.

Data Collection			
Complex	$OspC_A$-B5	$OspC_B$	$OspC_K$
Space group	$P2_12_12$	$P2_1$	$P2_1$
Cell parameters: *a,b,c* (Å) / β (°)	54.7 / 139.8 / 205.7	42.9 / 44.1 / 68.8 / 103.8	52.3 / 52.3 / 116.7 / 92.5
BNL Beamline	21-ID-E	21-ID-E	21-ID-E
Resolution range [a,] (Å)	50-2.70 (2.75-2.70)	50-1.50 (1.53-1.50)	50-1.95 (1.98-1.95)
wavelength (Å)	0.979	0.979	0.979
No. of reflections	3988365	3312121	2685656
Average redundancy[a]	2.8 (2.7)	2.7 (2.4)	2.8 (2.6)
$(I)/(\delta)$[a]	21.1 (1.2)	31.5 (3.2)	17.6 (1.7)
Completeness[a] (%)	99.6 (99.6)	95.8 (95.6)	97.8 (99.2)
R_{merge} [a,b] (%)	8.3 (145.0)	5.9 (32.5)	14.9 (131.1)
$CC^{1/2}$ [a,c]	(0.50)	(0.93)	(0.54)
Refinement			
Bragg spacings [a,] (Å)	49.4-2.7 (2.76-2.70)	36.8-1.5 (1.54-1.50)	39.7-1.95 (1.99-1.95)
R^d / R_{free} [e] (%)	20.4 / 25.6	14.7 / 16.7	19.3 / 22.8
No. of Protein atoms	8825	4908	4708
No. of Waters	32	270	358
RMSD bond length (Å)	0.005	0.012	0.003
RMSD bond angle (°)	0.78	1.14	0.52
Ramachandran favored / allowed[f] (%)	94.8 / 99.8	97.4 / 100	97.0 / 100
PDB code	**7UIJ**	**7UJ2**	**7UJ6**

[a] Values in outermost shell are given in parentheses.
[b] $R_{merge} = (\sum | I_i - \langle I_i \rangle |)/\sum | I_i |$, where I_i is the integrated intensity of a given reflection.
[c] $CC_{1/2} = (1+q^2\sigma_\varepsilon^2/\langle I \rangle 2^{-1}$, where σ_ε denotes the mean error within a half-datase, $CC_{1/2}$ is the correlation coefficient of two split data sets each derived by averaging half of the observations for a given reflection.
[d] $R = \sum | |F_o| - |F_c| | / \sum | |F_o| |$, where F_o and F_c denote observe and calculated structure factors, respectively.
[e] R_{free} was calculated using 5% of data excluded from refinement.
[f] Calculated using Molprobity.

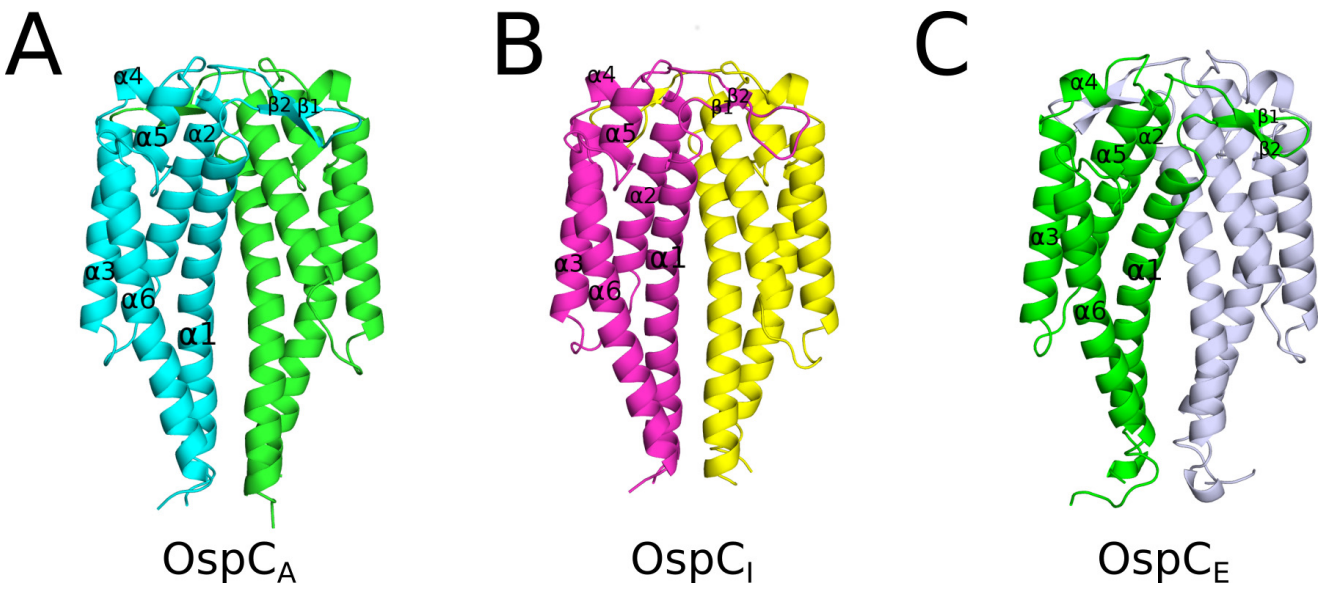

Figure S1. Structures of OspC types A, I and E. (A) Previously reported OspC structures. Ribbon diagrams of (A) OspC$_A$ [PDB ID **1GGQ**] colored green and cyan,; (B) OspC$_I$ [PDB ID **1F1M**] colored yellow and magenta; (C) OspC$_E$ [PDB ID **1G5Z**] colored light blue and dark green. All α-helices (1-6) and β-strands 1 and 2 are labelled highlighting structural similarity.

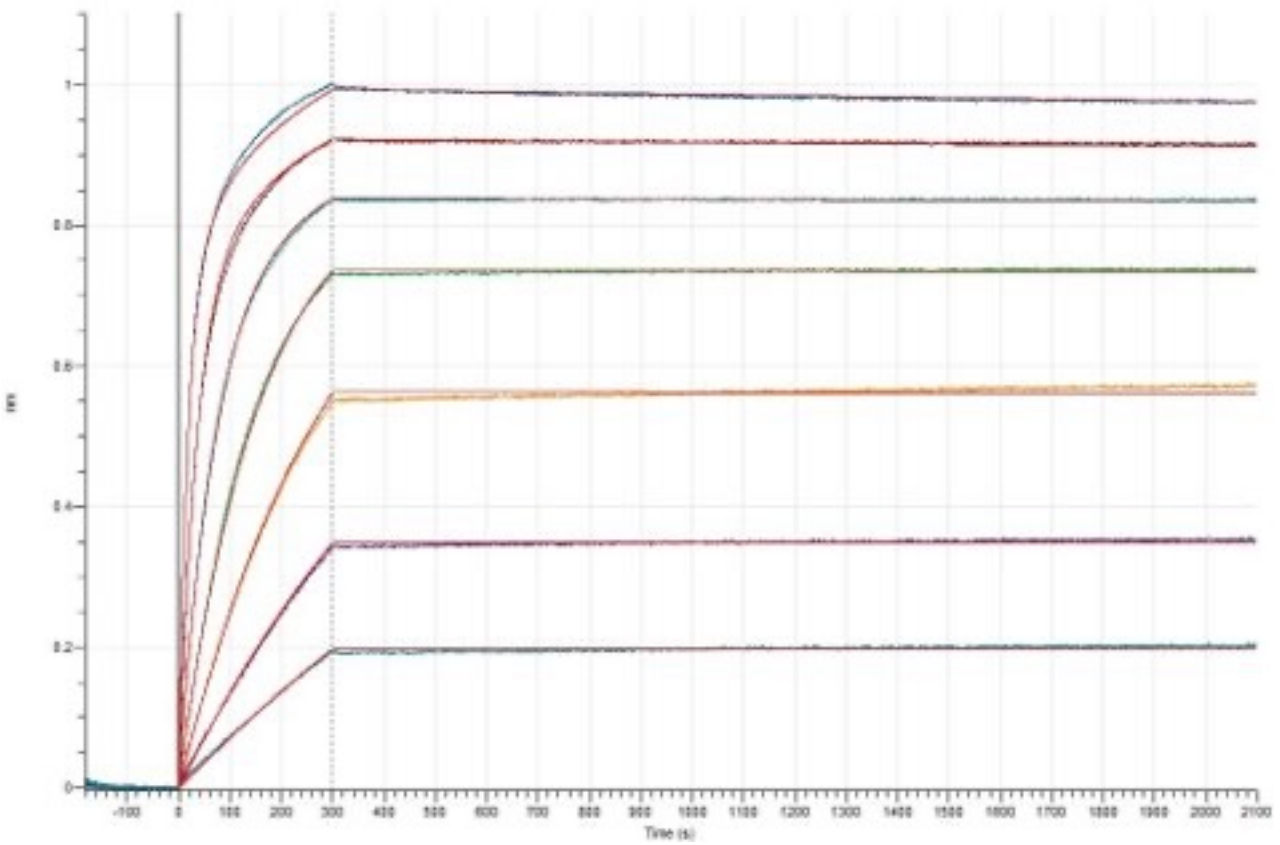

Figure S2. Representative B5-OspC BLI sensorgram. Biotinylated $OspC_A$ (3 μg/mL) in buffer (PBS containing 2% w/v BSA) was captured onto streptavidin biosensors, then exposed to a 2-fold serial dilutions (100 to 1.56 nM) for 5 min then 30 min dissociation, as detailed in the Materials and Methods. Results were analyzed using Data Analysis HT 12.0 software, and fit to a 1:2 bivalent analyte model.

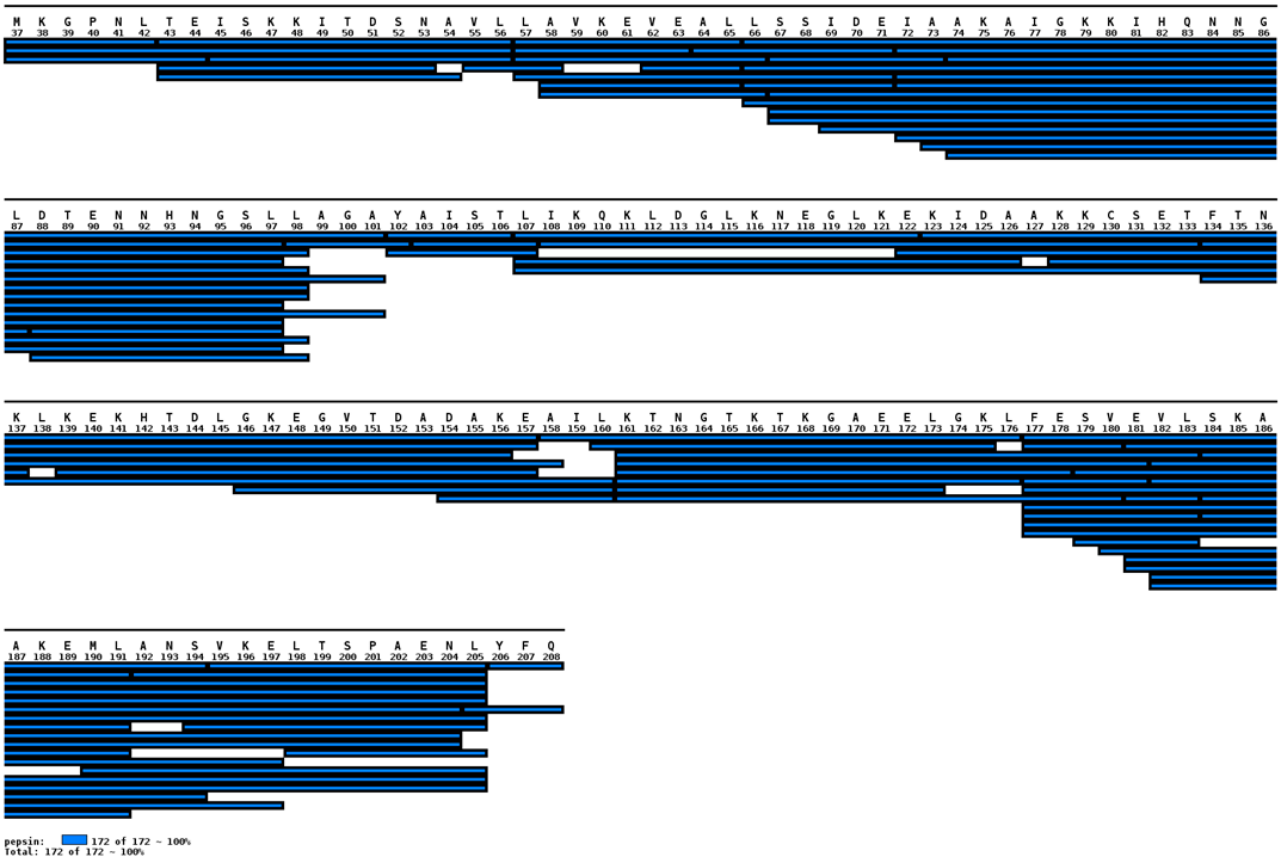

Figure S3. Platformed peptidic map of OspC_A. OspC_A was digested by in house prepared immobilized pepsin column (2.1×50 mm). Digested peptides were by trapped and desalted by C-8 column for 120 s and separated by a C-18 column,. For LC, mobile phase A was 0.1% formic acid in water, and B was 0.1% formic acid in acetonitrile. A total of 25 min LC method, 10 minutes with 15%-35%B was used to separate peptides, as described in the Materials and Methods. A total of 87 peptides were identified and mapped for OspC_A.

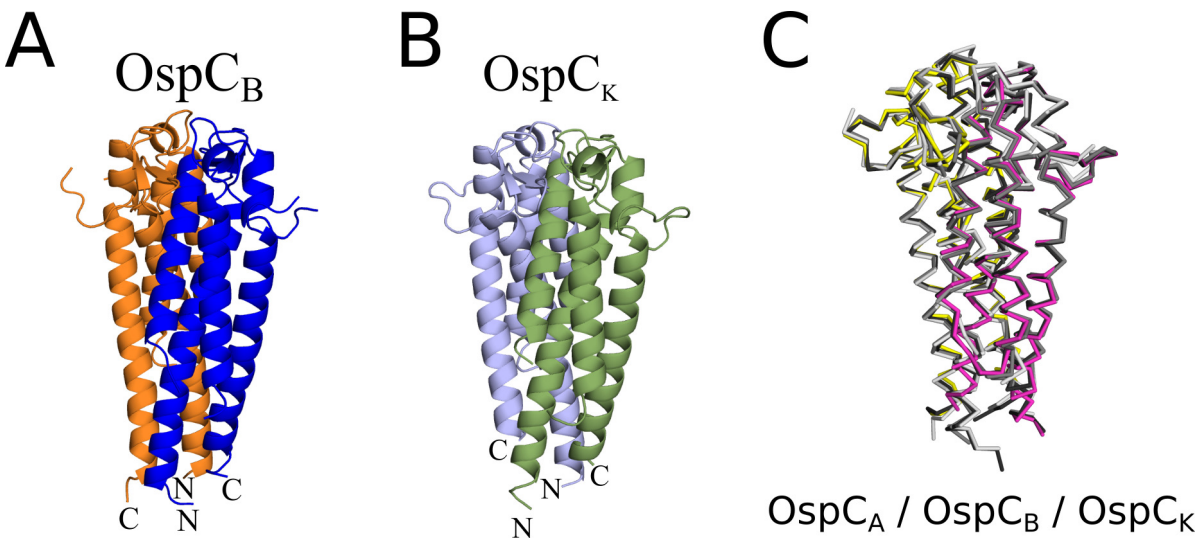

Figure S4. Structural comparison of OspC$_B$ and OspC$_K$ with OspC$_A$. Structures of (A) OspC$_B$ (blue and orange), and (B) OspC$_K$ (green and slate blue) depicted as ribbon diagrams with N- and C-termini labelled. (C) C-α traces of OspC$_A$ homodimer from the B5-OspC$_A$ complex (magenta and yellow) superpositioned with unbound OspC$_A$ (PDB ID: 1GGQ) colored dark gray, OspC$_B$ colored medium gray, and OspC$_K$ light gray.

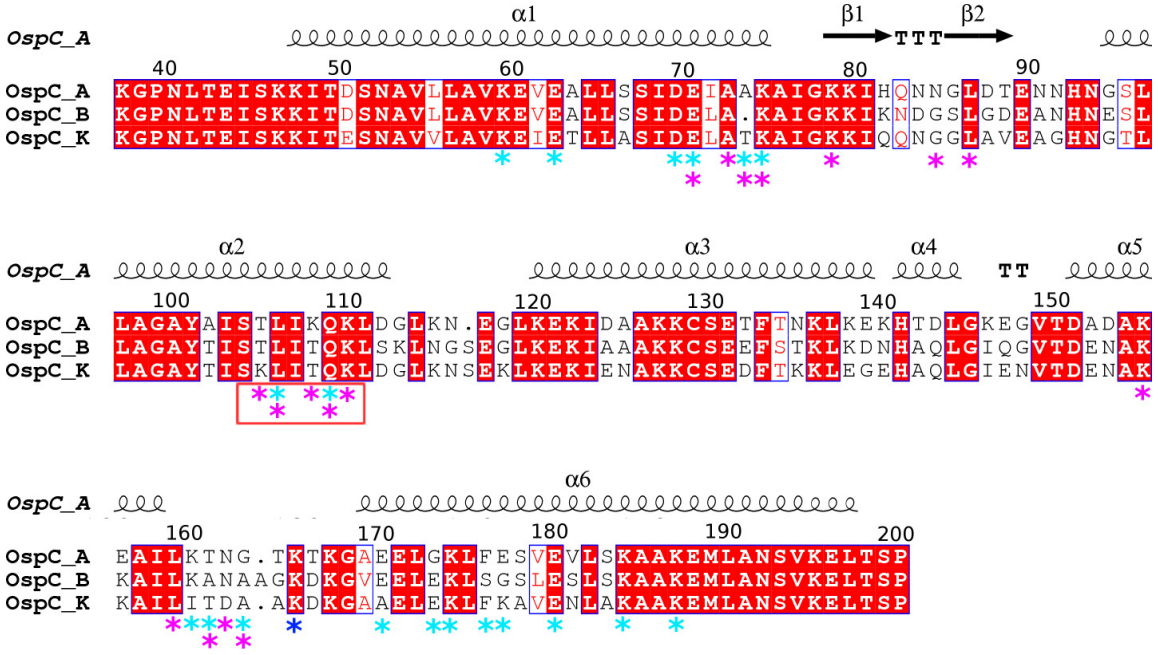

Figure S5. Sequence alignment of OspC A, B, K. Sequence alignment of OspC types A, B, and K from *B. burgdorferi* depicting the B5-interacting region of $OspC_A$. Magenta asterisks depict B5 V_L (L1-L3) interacting residues, cyan asterisks depict B5 V_H (H1-H3) interacting residues, and blue asterisks denote interaction with B5 V_L and V_H framework region residues. Secondary structural elements from $OspC_A$ bound to B5 are illustrated with α-helices 1-6 drawn as black coils and β-strands 1-2 drawn as black arrows above the sequence and labelled accordingly. Red background with white letters connotes sequence identity, white background with red letters connotes sequence similarity. The orange box below sequence region 100-110 shows B5 contact with the second $OspC_A$ monomer. Figure made with ClustalW and ESPript 3.0, as described in the Materials and Methods.

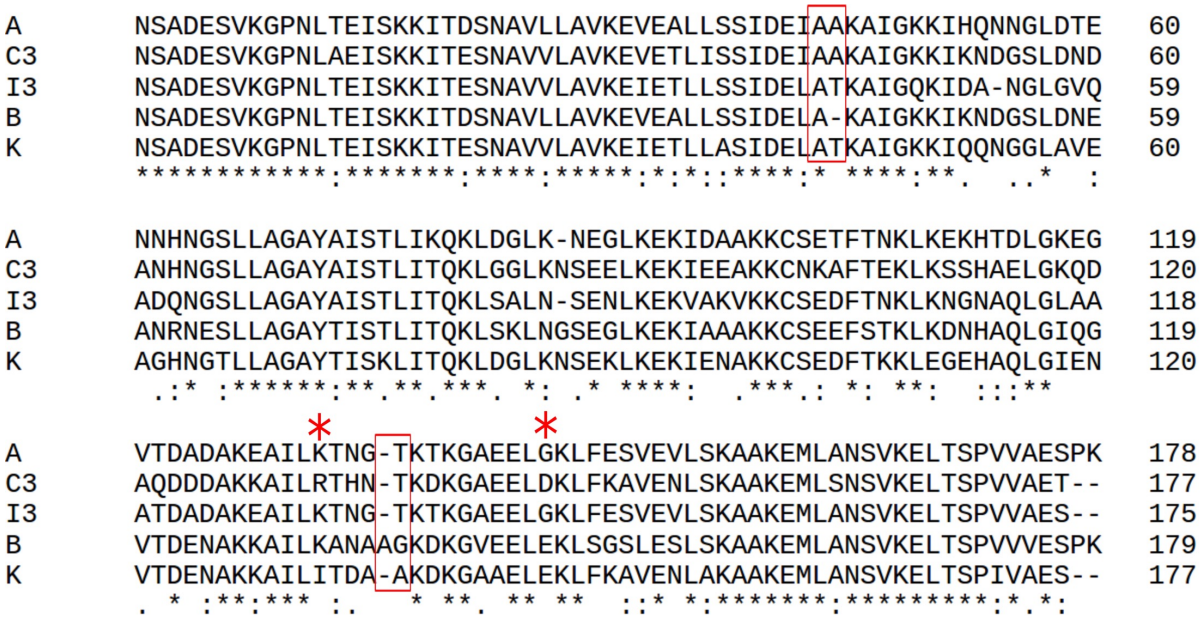

Figure S6. Sequence alignment of OspC types that conceivably bind B5. Primary sequence alignment of OspC types C3 and I3 with $OspC_{A,}$ $OspC_B$, and $OspC_K$ highlighting the key sequence similarities of $OspC_{C3}$ and $OspC_{I3}$ to $OspC_A$. Red rectangles encapsulate critical residues in α–helix 1 and loop 5-6 highlighting the insertion at residue 74 and deletion at residue 165 in $OspC_B$ that antagonize B5 binding. Red asterisks above the sequence identify the critical $OspC_A$ residues 161 and 175 which support interaction with B5. Black asterisks below the sequence denote sequence identity with two dots and one dot showing relatively reduced sequence similarity. Figure made with Clustal Omega.